Fluorescent dyes with large Stokes shifts for super-resolution optical microscopy of biological objects: a review

2015 Methods Appl. Fluoresc. 3 042004

(http://iopscience.iop.org/2050-6120/3/4/042004)

IOP Publishing Methods Appl. Fluoresc. 3 (2015) 042004 doi:10.1088/2050-6120/3/4/042004

Methods and Applications in Fluorescence

TOPICAL REVIEW

Fluorescent dyes with large Stokes shifts for super-resolution optical microscopy of biological objects: a review

Maksim V Sednev, Vladimir N Belov and Stefan W Hell

Department of NanoBiophotonics, Max Planck Institute for Biophysical Chemistry, Am Fassberg 11, 37077 Göttingen, Germany

E-mail: vbelov@gwdg.de

RECEIVED
17 April 2015

REVISED
28 August 2015

ACCEPTED FOR PUBLICATION
2 September 2015

PUBLISHED
22 October 2015

Keywords: fluorescence, dyes, large Stokes shift, STED microscopy

Abstract

The review deals with commercially available organic dyes possessing large Stokes shifts and their applications as fluorescent labels in optical microscopy based on stimulated emission depletion (STED). STED microscopy breaks Abbe's diffraction barrier and provides optical resolution beyond the diffraction limit. STED microscopy is non-invasive and requires photostable fluorescent markers attached to biomolecules or other objects of interest. Up to now, in most biology-related STED experiments, bright and photoresistant dyes with small Stokes shifts of 20–40 nm were used. The rapid progress in STED microscopy showed that organic fluorophores possessing large Stokes shifts are indispensable in multi-color super-resolution techniques. The ultimate result of the imaging relies on the optimal combination of a dye, the bio-conjugation procedure and the performance of the optical microscope. Modern bioconjugation methods, basics of STED microscopy, as well as structures and spectral properties of the presently available fluorescent markers are reviewed and discussed. In particular, the spectral properties of the commercial dyes are tabulated and correlated with the available depletion wavelengths found in STED microscopes produced by LEICA Microsytems, Abberior Instruments and Picoquant GmbH.

Main principles of super-resolution optical microscopy based on stimulated emission depletion (STED)

The fundamental physical phenomenon known as the Abbe diffraction barrier limited the optical resolution in conventional fluorescence microscopy to about 200 nm in the focal plane. Optical microscopes use visible focused light in the range of 400 − 800 nm and, according to the Abbe's law, the submicron scale cell structures (for example, cristae of a mitochondrion) could not be sufficiently resolved. However, recent discoveries and innovations resulted in new super-resolution techniques that allowed to surpass the diffraction barrier. For the pioneering inventions breaking the diffraction barrier, Stefan W Hell, William E Moerner and Eric Betzig received the Nobel Prize in Chemistry 2014. The present review describes fluorescent dyes with large Stokes shifts and their use in super-resolution optical microscopy providing resolution which is not limited by diffraction. The first part of the review deals with the basic principles of STED microscopy [1–3], because this super-resolution imaging method involves dyes with large Stokes shifts.

In STED, as well as in conventional fluorescence microscopy, focused light is used for the excitation of fluorophores in a diffraction limited size spot (see figure 1). In the case of STED microscopy, a red-shifted doughnut-shaped STED pulse is applied immediately after the excitation pulse. It features zero intensity only at the very center and thus depletes the excited state of the fluorophores at the periphery of the excitation spot by stimulated emission (induced $S_1 \rightarrow S_0$ transition).

In order to 'squeeze' the central spot efficiently, the depletion rate should exceed the rate of spontaneous transition to the ground state ($S_1 \rightarrow S_0$). Typical values of fluorescence lifetimes for organic fluorophores ($\tau_{fl} \sim 10^{-9}$ s) and optical cross-sections for their $S_0 \rightarrow S_1$ transitions ($\sigma \sim 10^{-16}$ cm^2) imply that intensity of STED pulse $I_{STED} >> I_S = (\sigma\tau_{fl})^{-1} \approx 10$ MW cm^{-2}, where I_S is the effective saturation intensity which can be defined as the intensity at which the probability of fluorescence is reduced by half. The optical resolution in STED is defined by equation (1).

$$d \approx \frac{\lambda}{2n \sin\theta \sqrt{1 + I_{STED}/I_S}} = \frac{d_c}{\sqrt{1 + I_{STED}/I_S}}. \quad (1)$$

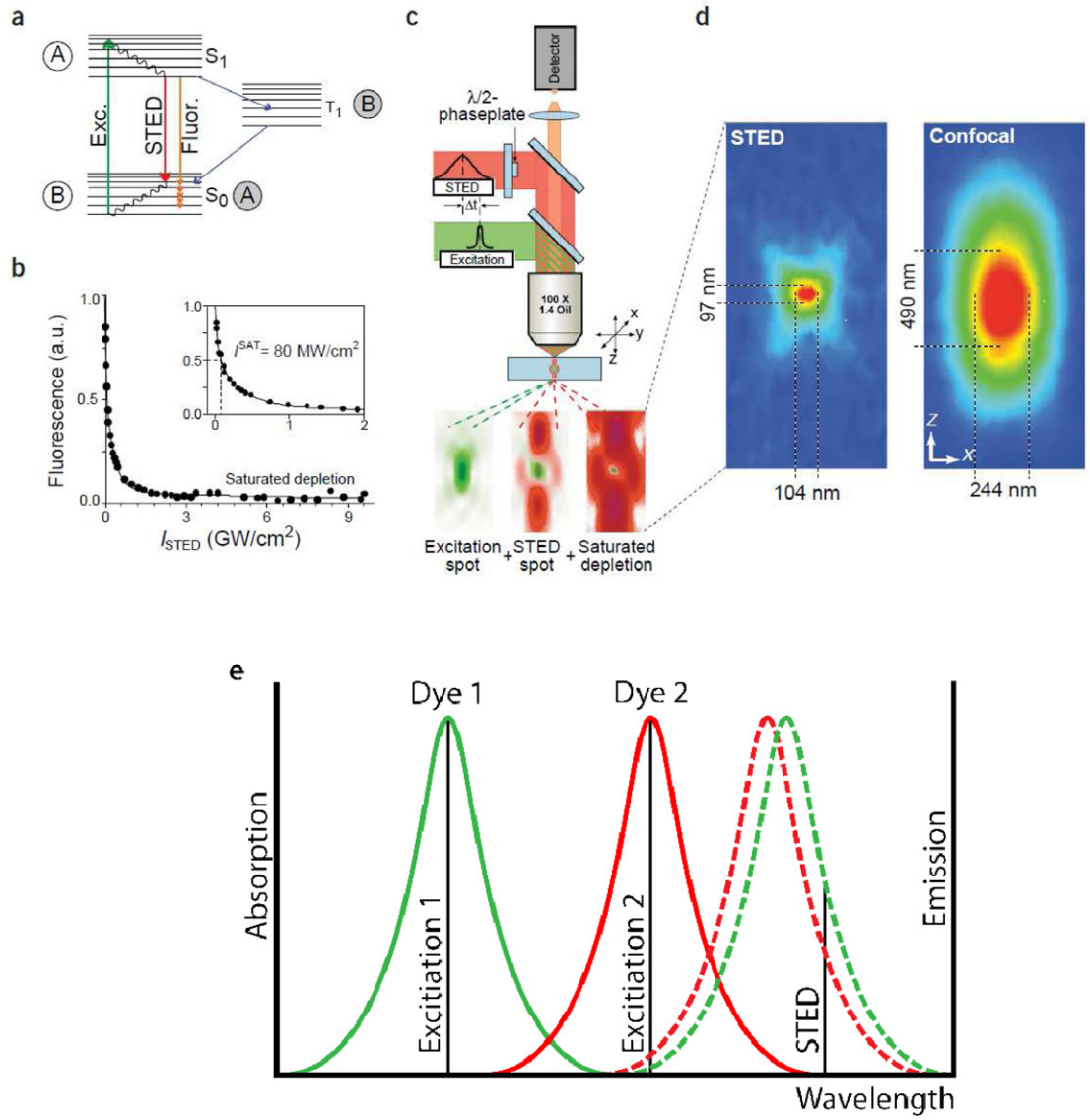

Figure 1. Physical conditions, setup scheme, typical focal spot and two-color imaging scheme for STED microscopy [4]: (a) energy diagram of an organic fluorophore; (b) depletion of the excited state S_1 with a STED pulse of increasing intensity (I_{STED}); (c) sketch of a point-scanning STED microscope; (d) fluorescent spots in the STED and confocal microscopes; (e) absorption spectra (continuous lines) and emission spectra (broken lines) of a large Stokes shift dye (green) and a dye with a small Stokes shift (red); both dyes can be depleted with one wavelength (STED).

The value $d_c = \lambda/2n \sin\theta$ (θ—semi-aperture angle) represents the resolution of a diffraction-limited system. According to equation (1), a significant improvement in resolution can be achieved only at very high powers of the I_{STED} pulse. Such enormous light intensities (>100 MW cm^{-2}) inevitably cause photobleaching of the fluorophores, and therefore only photostable dyes are suitable for STED microscopy of highest resolution (<30 nm). In addition, to increase the sensitivity and reduce the imaging time, fluorophores with high fluorescent quantum yields are required.

One of the main advantages of fluorescence microscopy is the ability to use several fluorescent labels to target different specimens and produce multicolor images that help to identify many structural features of biological objects and interactions between them. For multicolor imaging experiments, the spectral separation of different labels into two or more excitation or detection channels is required. In this regard, fluorophores with large Stokes shifts are particularly valuable, because they allow reducing the number of detection channels, avoiding cross-talk and simplifying the imaging scheme of a multicolor experiment (figure 1(e)). For example, two-color STED microscopy (2C STED) can be easily realized if we combine fluorescent dyes with small (10 − 30 nm) and large (>80 nm) Stokes shifts. If the emission spectra of these dyes overlap, two different excitation wavelengths can be used to distinguish them (see figure 1(e) and final sections of this review). At the same time, due to similar emission spectra, only one STED beam is needed for both dyes. The powerful STED light can cause re-excitation of the dye with small Stokes shift (figure 1(e)). This phenomenon is undesired, because re-excitation produces a diffuse halo around the sharp super-resolution image. In this respect, dyes with large Stokes shifts are advantageous,

as they cannot be excited by STED light (figure 1(e)). For achieving the best image quality and optical resolution in the range of 30–40 nm, special attention should be given to the sample preparation which is particularly important in STED microscopy [5].

The duration of the excitation pulse is less than 50 ps; the STED pulse follows or even overlaps to some extent with the excitation pulse and is 200–300 ps long (without gated STED), or about 1 ns long (in the case of gated STED). For the green fluorescent protein, it was shown that the depletion is efficient, even if the wavelength of a STED beam overlies the absorption band in the spectrum of the excited state [6]. However, in this case excitation to higher energy levels is likely to occur. It may cause photobleaching of the dye, because higher excited states are more chemically reactive than S_1 or S_0 states. Unfortunately, the excited states spectra of the STED dyes have not yet been studied. The understanding of these spectra could probably help to create more photostable and efficient STED dyes.

The drawback of many fluorescent dyes with large Stokes shifts is their relatively low brightness (product of the molar extinction coefficient and fluorescence quantum yield) and poor photostability. Fast photobleaching under very powerful STED light is the major problem which limits the use of most dyes with large Stokes shifts in STED microscopy of highest nanometric resolution. This so called structured illumination microscopy (SIM) [7, 8] offers a resolution of only about 100 nm representing a two-fold improvement compared with the confocal method. The method of SIM tolerates the use of less photostable fluorophores than those required in STED nanoscopy at the same low (∼100 nm) resolution. All dyes with large Stokes shifts (see table 1) can then be used.

Overview of the labeling and bioconjugation techniques

Fluorescence microscopy is one of the most important techniques in physical, chemical, and biological studies of living and fixed cells, tissues, or even whole organisms [9–34]. A vast majority of all microscopy investigations is performed with conventional lenses and visible light, despite the significant achievements made by electron- and x-ray microscopies. Biological tissues are transparent to visible light to a great extent. This inherent property is advantageous for fluorescence microscopy and provides the possibility of non-invasive imaging in 3D applied to the interior of cells. Furthermore, various cellular constituents, such as proteins, nucleic acids or lipids, can be detected specifically with fluorescence tagging. Selective, sensitive and reproducible imaging of the target objects depends on the optimal combination of several chemical, biological and physical factors. The availability and proper choice of fluorescent markers—fluorescent proteins or synthetic fluorescent dyes—plays an important and often decisive part in the whole labeling and imaging sequence. The present review deals with synthetic fluorescent dyes possessing large Stokes shifts and their use in optical super-resolution microscopy. In this section we briefly review the important bioconjugation methods applicable to all fluorescent dyes, including fluorochromes with large Stokes shifts.

All fluorescent labels have to be specifically bound with the target biological objects—proteins (peptides), carbohydrates, lipids, nucleic acids, (modified) oligonucleotides, toxins, various 'small' molecules as 'recognition units', etc. The bioconjugation procedures require fluorescent dyes with reactive groups which specifically interact with the target and efficiently attach the fluorescence label to the required object [35]. The classical and most robust labeling approach is indirect immunofluorescence [36–40]. In this method the object (antigen) is recognized and bound by the externally applied primary antibody which, at the next step of the labeling procedure, forms a very stable complex with one or several secondary antibodies. These secondary antibodies have to be pre-labeled with the required fluorescent dye [35, 41]. Primary and secondary antibodies are raised in animals—mice, rabbits, goats, donkeys, etc. For example, the secondary goat anti-mouse antibodies are formed in goat against primary antibodies obtained from mouse as an immune response to the target antigen. The advantage of this approach is that only one type of secondary antibody is sufficient to bind with many types of primary antibodies, provided that (for an example mentioned above) they were raised in mice against various antigens. This reduces the amount of work and simplifies the labeling procedure, because one type of secondary antibody can be easily marked with various fluorescent dyes, rather than labeling various types of primary antibodies with various dyes. The indirect immunofluorescence can provide an additional degree of amplification of the fluorescence signal, because one primary antibody can form stable complexes with more than one secondary antibody. Typically, the most common antibodies (Immunoglubulins G, IgG) consist of several protein domains bound with disulfide bonds; their molecular masses are 150–170 kDa [36–40], and their size is about 8 nm [42]. Therefore, formation of primary–secondary antibody clusters increases the dimensions of the labeled biological entity. This increase in size has to be taken into account when considering the quantitative results obtained in the course of imaging using diffraction unlimited optical microscopy. Immunofluorescence is applicable only to dead (and fixed) cells, because antibodies cannot cross the cell membrane. In order to deliver antibodies into the inner parts of the cells, special techniques, like electroporation or the use of detergents (Triton X100) as permeabilizing agents, have to be applied. On the other hand, proteins in the outer plasma membrane of the living cells can be labeled with antibodies (pre-stained with fluorescent

dyes). All super-resolution imaging results obtained up to now with the fluorescent dyes possessing large Stokes shifts involved indirect immunofluorescence as the labeling procedure.

The progress in modern bioconjugation techniques and, in particular, in immunofluorescence resulted in many novel methods and approaches. Recently, single-domain antibodies ('nanobodies') having molecular masses of about 15 kDa emerged as an alternative to traditional antibodies [43]. Nanobodies were shown to be applicable in super-resolution optical microscopy and, due to small size, provide more adequate evaluation of the dimensions of biological objects (e.g. the diameter of a microtubule) [44]. Though this study was based on a super-resolution method which has not (yet) been applied to fluorescent dyes with large Stokes shifts, it demonstrated for the first time that small nanobodies preserved their binding efficiency upon labeling with the relatively bulky (cyanine) dyes. In this context it is important to mention that the degree of labeling (DOL)—average number of dye residues attached to one protein molecule—represents an important parameter in immunofluorescence labeling with antibodies and nanobodies [35–39, 42]. There is an optimal DOL value in respect of maximal brightness provided in the course of immunostaining. Too many dye residues (>3–6 depending on the dye polarity) attached to one protein molecule may cause quenching of the fluorescence signal due to formation of the non-emitting aggregates and/or the energy-transfer (homo FRET effect). In this respect, it is important to control DOL values using classical methods [35–39], as well as statistics of multiple photon detection events [45], and also determine the fluorescence quantum yields of the dye conjugates.

Unfortunately, immunofluorescence in fixed cells may produce artifacts. Moreover, fixatives and cell-permeabilizing agents may even cause protein extraction and relocalization [46]. Therefore, it is important to combine immunofluorescence with live-cell imaging. However, nanobodies themselves (without attaching cell penetrating peptides) do not pass through cell membranes. Thus, new labeling strategies were required for implementation of the super-resolution optical microscopy in living cells. We discuss these new labeling techniques related to the living cells very briefly, because they have not yet been combined with the use of fluorescent dyes possessing large Stokes shifts. However, in the upcoming labeling and imaging of living cells, it will be important to combine 'normal' dyes with fluorochromes possessing large Stokes shifts (for the reasons discussed below).

In recent years, several novel site specific labeling protocols for proteins were invented and developed [47–53]. The main breakthrough in this approach is based on the possibility to fuse genetically (to 'tag') the protein of interest with a new small protein (enzyme) which is able to selectively and very rapidly form a new covalent bond with a substrate. If a substrate—a small molecule—will be attached to a fluorescent dye (or other label) and delivered into living cells, it could react with an enzymatic part of the tagged protein providing the site specific labeling. For example, the SNAP-tag is a small protein based on human O^6-alkylguanine-DNA-alkyltransferase (hAGT), a DNA repair protein [47–51]. The SNAP-tag substrates are guanine or chloropyrimidine derivatives bound with dyes, biotin, other markers or even surfaces via a benzyl linker. In the course of the labeling reaction, the substituted benzyl group of the substrate selectively and rapidly reacts (in an S_N2 fashion) with the SNAP-tag and forms a stable chemical bond with a protein of interest (via the SNAP tag) [51]. The site-specific labeling does not work equally well with all fluorescent dyes, because the dye can influence the binding efficiency and recognition parameters of the substrate to a great extent. Fluorescent dyes with complex structures may not fit the binding pocket in an enzyme. If the fusion proteins derived from Halo- [52, 53], SNAP-, CLIP- [47–51] or other tags are situated inside (living) cells, then their substrates (recognition unit + label) have to be cell-permeable. This is a very important feature which severely restricts the variety of applicable fluorescent dyes. In general, they have to be neutral (or zwitterionic with a short charge separation distance and a zero net charge), possess a compact structure, limited molecular mass ($M < 800$ Da), and medium polarity (several heteroatoms as hydrogen bond donors and acceptors). Importantly, many coumarins—dyes with large Stokes shifts—fulfill all these requirements and therefore are expected to be able to cross membranes of living cells. Thus, fluorescent coumarins are promising dyes for testing their ability of binding with the genetically encoded protein tags.

Quite recently, novel labeling techniques have emerged [54–56]. They are based on the so-called 'click-chemistry' transformations, very rapid and selective second-order reactions binding two chemical entities with each other. For example, in the presence of copper(I) salts as catalysts, alkynes (compounds having a triple bond C≡C) readily react with organic azides (RN_3) forming five-membered heterocycles—1,2,3-triazoles. Azide or alkyne residues can be integrated into amino acids, and these (unnatural) amino acids can even be site-specifically incorporated into proteins in cells in response to the TAG codon [57]. However, the main disadvantage of this approach is that it relies on copper(I) salts which may be toxic to cells. The strained alkynes with 8-membered ring incorporating C≡C triple bond were proposed as more reactive derivatives. This kind of strain-promoted alkyne–azide cycloaddition afforded in the best cases the second order rate constants in the range of 0.1–1 $M^{-1}\,s^{-1}$ [54–56]. A further, crucial improvement in the kinetics was achieved, when strained alkenes (norbornene or *trans*-cyclooctene derivatives) reacted with 3,6-diaryltetrazines. This transformation can be understood as an inverse electron-demand Diels-Alder (ieDA) cycloaddition,

in which the tetrazine component can be considered as a diene, and the strained alkene—as a dienophile. At the first step, the unstable polycyclic intermediate is formed, which loses the nitrogen molecule, forms 1,5-dihydropyridazine derivative, and, finally, tautomerizes into the stable 1,4-dihydropyridazine product. The reaction between biomolecules decorated with norbornene residues (e.g. proteins with incorporated ω-(norbornyloxycarbonyl) lysine residues) and commercially available fluorescent dyes bearing 3-phenyltetrazine groups has the rate constant (k_2) of about $2\,M^{-1}\,s^{-1}$. In the case of trans-cyclooctenes as strained systems, the reaction rates are much higher ($k_2 > 100\,M^{-1}\,s^{-1}$). These examples show that the continuous progress in bioconjugation methods requires fluorescent dyes with new and unconventional reactive groups. In these dyes, the length and art of linker may also be very important [32]. In addition, the aptamer binding represent a promising bioconjugation technique [58, 59].

Fluorophores with large Stokes shifts caused by intramolecular charge transfer (ICT)

Photostable and bright fluorescent dyes with large Stokes shifts are rare and only few are commercially available. Nearly all these dyes contain the coumarin fragment as the fluorophore. For example, 'Mega Stokes' dyes from Dyomics are coumarins absorbing at about 500–520 nm, and emitting in the region of 590–670 nm (in ethanol). Another practically useful coumarine dye is AlexaFluor™ 430 with absorption and emission maxima at 434 nm and 539 nm, respectively (see table 1). Many other providers (e.g. Life Technologies, BD Biosciences, Active Motif, Atto Tec GmbH, etc) offer fluorescent dyes or their conjugates with large Stokes shifts, but they often do not publish their structures. For example, the structures of Pacific Orange™ (abs. 390 nm, emission 540 nm; Invitrogen) and BD Horizon™ V500 (abs. 415 nm, emission 500 nm; BD Biosciences) have not been disclosed. The lack of essential structural data hinders the proper choice of the fluorescent dye for a particular biochemical application (for example, due to the indefinite hydrophilicity, unknown net electrical charge of the molecule, and potential (photo)toxicity). Unavailable structures of the popular and frequently used dyes hamper the progress in basic research aimed at the creation of new fluorophores. This is particularly true for the coumarins, whose common features are moderate photostability and relatively low fluorescence quantum yields in polar solvents. Low photostability of coumarins (in comparison with xanthenes and other photostable fluorochromes) can be explained by the relatively high probability of the transition to the triplet state upon excitation [60]. The lack of brightness and low photoresistance are the main drawbacks which preclude their wide use in modern optical 'nanoscopy' [61–64]. These novel super-resolution methods of the far-field optical microscopy require fluorescent dyes which demonstrate all advantages and full scope of the new physical concepts. Therefore, the analysis of the available structures, spectra, fluorescence quantum yields, solubility in aqueous buffers, and chemical reactivity with various biologically relevant targets is an important prerequisite for choosing the best dye for a given labeling and imaging procedure.

Despite the significant advances in quantum-mechanical methods, it is still impossible to predict accurately all important properties of fluorescent dyes, such as band shapes, maxima of absorption and emission spectra in different solvents, Stokes shifts, molar extinction coefficients and fluorescence quantum yields. In most cases, the dipole moment of a fluorophore in the excited state differs from that in the ground state. Therefore, after excitation, the solvent dipoles that surround a molecule of the fluorophore may rearrange, leading to a better stabilized excited state with lower energy. If the dipole moment of the dye molecule in the excited state is higher than the dipole moment of the same dye in the ground state and the solvent polarity increases, then the energy of the excited state becomes lower. As a result, the emission spectra exhibit a red-shift in more polar solvents. Geometrical relaxation in the excited state and rearrangement of the solvent dipoles (relaxation of the solvent media) are two photophysical processes responsible for the value of the Stokes shift. Thus, in order to increase the Stokes shift, one could try to predict and design structures with large differences between the equilibrated geometries and dipole moments in the ground and excited states.

Unfortunately, these differences are difficult to predict. As a consequence, the design of the new fluorophores and even the choice of optimal dye from the set of commercially available markers still remains mostly a matter of trial and error. Therefore, the users have to analyze first of all the known data for commercially available substances (table 1), taking into consideration general and often empirical guidelines. For example, the intramolecular charge transfer (ICT) in the excited state is very often responsible for the large Stokes shift. Stronger or weaker acceptors and/or donors, or even new π-systems can be introduced to the core fluorophore in order to 'tune' the 'push–pull' electronic effect or expand the conjugation system of the dye, thus providing bathochromic and bathofluoric shifts and increasing molar extinction coefficient. However, the precise structure–property relationships are still unclear. A useful report generalizing these regularities and providing detailed guidelines for the design of certain classes of fluorophores has been published recently [65]. Apart from ICT and relaxation of solvent molecules around a fluorophore in the excited state which are considered as photophysical processes, such photochemical processes as excimer/exciplex formation, excited state intramolecular transfer (ESIPT) and twisted ICT (TICT) are also known to result in emis-

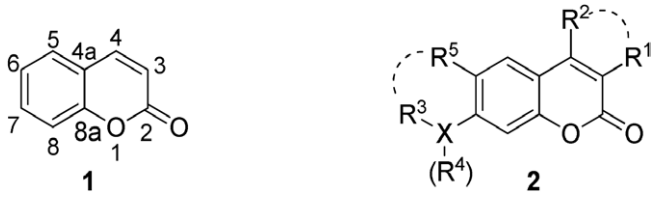

Figure 2. Parent coumarin **1** and the generic structure of fluorescent coumarin dyes **2**: R^1 = acceptor, $(CH_2)_nCOOH$, and/or heterocyclic residue; R^2 = H or acceptor group (e.g. CF_3, CN); X = N or O; R^4—linker, R^3, R^5 = H, alkyl, alkenyl, aromatic system, etc.

sion with a large Stokes shift [66]. As a rule, intensity of this emission is very low. In fact, these processes were also found to be responsible in many cases for quenching of fluorescence. For example, in the case of 7-*N*,*N*-dialkylaminocoumarins, where formation of the non-emissive TICT-state in polar solvents is associated with a dramatic decrease in fluorescence quantum yields [67–70].

Despite the very long history and wide use of coumarin dyes (figure 2), their structure–property relationships are not studied in depth [67, 70–89]. Large Stokes shifts in coumarins are provided by using intramolecular charge transfer (ICT) and (rarely) excited state intramolecular proton transfer (ESIPT) mechanisms [66]. Variously substituted coumarins (and hybrid dyes based on them) are probably most important fluorophores exhibiting large Stokes shift. Coumarin **1** itself (figure 2) shows no fluorescence at room temperature and has only weak absorption in the near UV region, but if C-6 or/and C-7 is substituted with an electron-donor group (such as hydroxyl or amino group), an intense blue–green emission appears. It originates due to a 'push–pull' effect between the electron-donor group(s) at C-6(7) and the electron-withdrawing lactone moiety.

The aldehyde group at C-3 in a coumarin enables to produce hybrids between coumarin and cyanine dyes. These novel far-red emitting fluorophores with large Stokes shifts are based on 7-dialkylaminocoumarins (e.g. DY-601XL in table 1) or 7-hydroxycoumarins. These hybrid dyes were decorated with hydrophilic residues. In the case of 7-hydroxycoumarins, quenching groups which may be cleaved-off by hydrolytic enzymes were attached to the phenolic hydroxyl. Thus, new 'masked' fluorescent dyes probing the activity of the highly efficient bio-catalysts were created [84]. A similar approach was used in the course of creating the fluorimetric sensors for other enzymes or physiologically active thiols which trigger the (cascade) reactions and liberate the free hydroxyl group at C-7 (responsible for fluorescence) [85, 86, 88].

Coming back to the commercially available fluorophores which can be excited with visible light ($\lambda_{exc} \geqslant 400$ nm) and possess large Stokes shifts, we can state that *nearly* all of them contain the coumarin fragment. A few notable exceptions are represented by PyMPO (linearly extending heteroaromatic π-system with strong donor and acceptor groups), Lucifer Yellow (disulfonylated imide of 4-aminaphthalene 1,8-dicarboxylic acid), APTS (1-aminopyrene-3,6,8-trisulfonate), NBD-X (*N*-alkyl-4- amino-7-nitrobenz-2-oxa-1,3-diazol), propidium iodide, Atto 465 (*N*-(3-carboxypropyl)-3,6-diaminoacridinium), as well as Atto 430LS and 490LS dyes (presumably 2,7,9-tris-(alkylamino)xanthenes). Other dyes with large Stokes shifts may include benzooxazole or triphenylpyrazoline derivatives. Although these fluorophores have good fluorescence quantum yields, they require UV light for excitation, which is often incompatible with imaging biological samples. Examples of the commercially available coumarin dyes are given in table 1. The largest part of them belongs to the family of 7-aminocoumarins, with variable substituents in positions 3 and 4. (In most cases, the position 4 is unsubstituted.) The electron-acceptor group at position 3 with an extended π-system (e.g. *N*-alkyl-2-vinylpyridinium salt with $-M$-effect in compound DY-480XL) strongly shifts the absorption and emission bands to the red spectral region and increases the distance between their maxima. A very strong acceptor at position 4 (e.g. CF_3-group in AlexaFluor™ 430) with a negative inductive effect ($-M$) also increases the charge separation and the 'push–pull' character of the chromophore, and provides similar spectral shifts. Incorporation of the 7-amino group into the 2,2,4-trimethyl-1,2-dihydroquinoline ring (Alexa Fluor 430, DY-431, DY-510XL, DY-511XL, Abberior Stars 440 SXP, 470 SXP, and 520 SXP) or 2,2,4-trimethyl-1,2,3,4-tetrahydroquinoline ring (Atto 390, Atto 425) provides an additional small red-shift of 10 or 5 nm (compared with 7-dialkylamino group) and creates new variable positions: a methyl group at the double bond and the asymmetrically disubstituted nitrogen atom. These variable positions may be used to introduce the sulfonic acid groups (Alexa Fluor 430, DY-431, DY-511XL), phosphoric acid residues (Abberior Stars 440 SXP, 470 SXP, and 520 SXP) and ω-carboxyalkyl groups, respectively. Introduction of these polar groups do not change the positions of the absorption and emission bands (compared with the parent non-polar dyes deprived of the ionic residues). However, more hydrophilic derivatives have higher fluorescence quantum yields (as free dyes and in bioconjugates) in aqueous solutions and perform better in optical microscopy. They bind more specifically with the target structures (do not 'stick' to lipophilic domains in biomolecules) and provide less fluorescent back-

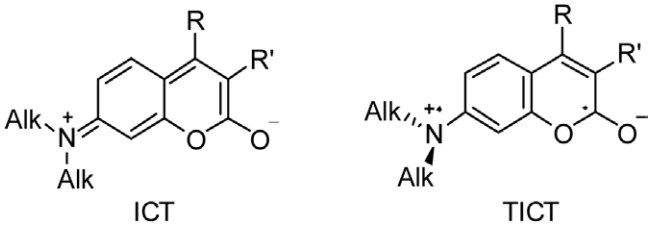

Figure 3. 'Normal' intramolecular charge transfer (ICT) and twisted intramolecular charge transfer (TICT) excited states of 7-*N*,*N*-dialkylaminocoumarins.

ground in images. An additional functional group (e.g. COOH) is always required for conjugation reactions. Phosphorylated Abberior Star dyes (440 SXP, 470 SXP, and 520 SXP) demonstrate higher fluorescence quantum yields in conjugates, compared to the corresponding sulfonated analogues [90, 91]. The betain fragment in Abberior Star 520 SXP provides a batochromic shift of absorption and emission bands (compared with the 'parent' dye Abberior Star 440 SXP), and further increases the Stokes shift, but the fluorescence quantum yield in aqueous solutions decreases (see table 1). This is a general rule for all fluorescent dyes: increase in the Stokes shift is accompanied with a decrease in the fluorescence quantum yield. A variation of the substituent at C-4 in the coumarin system is another tool which enables to 'tune' the positions of the absorption bands. In particular, the presence of CF_3-group at C-4 in Alexa Fluor 430 and Abberior Star 470 SXP dyes provides strong bathochromic and bathofluoric shifts and increases the separation between the absorption and emission bands (compared with analogs without any substituents at C-4). In addition, the introduction of trifluoromethyl group to C-4 was found to reduce photobleaching by 20% in coumarin dyes [92].

7-Hydroxycoumarins are emissive only in their anionic forms, and this makes them unattractive for applications at physiological pH values: these compounds will be neutral and, therefore, nonfluorescent. A great improvement is 6,8-difluoro-7-hydroxycoumarin—Pacific Blue—with reduced pK_a of 3.7 [93]. The greater acidity makes this dye predominantly anionic at physiological pH. However, the anionic nature of this fluorophore is undesirable in some cases [94]. In general, the anionic dyes and their conjugates with net electrical charge less than −1 are cell-impermeable. This rule is valid for all phosphorylated dyes and for many sulfonated compounds.

Dyomics GmbH designed various 7-N, N-dialkylaminocoumarins as 'MegaStokes' fluorescent dyes [95]. Most of them possess a *trans*-double bond between C-3 of the coumarin skeleton and the pyridinium moiety and absorb at about 500 − 515 nm (in EtOH) in the case of the 2-pyridinium substituent (DY-480XL and DY-481XL in table 1) and at about 509 − 523 nm (in EtOH) in the case of the 4-pyridinium substituent (compounds DyLight 510LS, DY-511XL, DY-520XL and DY-521XL). If we compare the structure of DY-511XL with the structures of DY-520XL and DY-521XL, we can conclude that the introduction of a sulfonic acid residue to the 4-alkylpyridinium ring and the presence of the freely rotating N,N-dialkylamino group in these dyes resulted in a small (10 − 13 nm) bathochromic shift and a large bathofluoric shift (60 nm). The presence of the 'non-aromatic' CH = CH-bond may have a negative effect on photostability, because this bond may be susceptible to photo-oxidation. This bond is not ultimately required for achieving the absorption at wavelengths >520 nm (excitation with 532 nm laser): for example Abberior Star 520 SXP dye has an absorption maximum at 522 nm (in aqueous PBS buffer), but it does not have CH = CH bond between C-3 in the coumarin scaffold and the 4-pyridinium group attached to it. However, the presence of additional conjugation unit (CH = CH bridge) provides larger Stokes shifts of 140 nm. 7-Diethylaminocoumarin-hemicyanine hybrid DY-601XL have the most red-shifted absorption maximum (606 nm in EtOH) in this series and emit in the near-IR region with a moderate Stokes shift of 57 nm ($\lambda_{max,em}$ = 663 nm).

As a rule, fluorescence efficiencies of 7-aminocoumarins decrease in highly polar solvents (e.g. in aqueous buffers). This reduction is particularly sharp, if the amino group is dialkylated and cannot form hydrogen bonds with solvent molecules. Upon excitation of the dyes with less rigid geometries followed by rotation of the amino groups, an internal conversion of the initial ICT state to a non-emissive twisted intramolecular charge-transfer (TICT) state with full charge separation may take place (see figure 3) [67, 69, 96]. This kind of state is stabilized by electron withdrawing groups at C-3 or C-4 and by electrostatic interaction with molecules of a polar solvent. As a result, coumarins with freely rotating 7-dialkylamino groups have poor fluorescence quantum yields in aqueous and alcoholic media. As expected, rigidization of the fluorophore by including the amino group into one or two rings fused with the π-system leads to considerable improvement in fluorescence efficiency, because in this case excitation yields a normal planar ICT state. It was also established that there is no need for rigidization, if the amino group carries only one alkyl group. The rigidized amino groups have lone electron pairs which overlap efficiently with the π-electron system of the dye. These 'planar' amino groups are stronger electron-donors than 'twisted'

Table 1. Selection of commercially available dyes with large Stokes shifts suitable for use in super-resolution light microscopy.

Name	Structure	$\lambda_{abs,max}$[a] (nm)	$\lambda_{em,max}$[b] (nm)	ε[c] (M^{-1} cm^{-1})	Additional information	Manufacturer
Indo-1	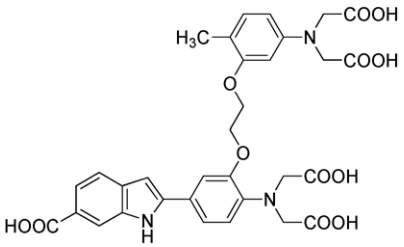				$\Phi_{fl} = 0.56$ (high Ca^{2+}) / 0.38 (zero Ca^{2+}) in H_2O[e]	
High calcium[d]		330	401	33 000	STED: 592 nm (gated CW; LEICA)[f]	Life Technologies
Zero calcium[d]		346	475	33 000	or 595 nm (pulsed; Abberior)[f]	
Fura-2	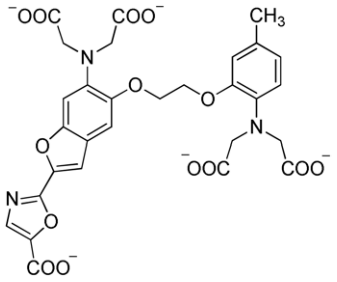				$\Phi_{fl} = 0.49$ (high Ca^{2+}) / 0.23 (zero Ca^{2+}) in H_2O[e]	
High calcium[d]		335	505	34 000	STED: 592 nm (gated CW; LEICA)[f]	Life Technologies
Zero calcium[d]		363	512	28 000	or 595 nm (pulsed; Abberior)[f]	
AMCA, succinimidyl ester	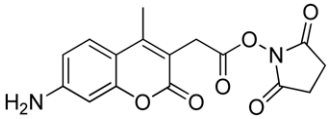	345	440	19 000	—	Life Technologies
CF 350	—	347	448	18 000	in H_2O	Biotium
DY-350XL	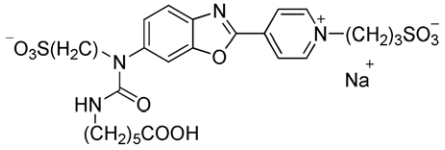	349	610	16 000	in EtOH	Dyomics GmbH

(*Continued*)

Table 1. (*Continued*)

Name	Structure	$\lambda_{abs,max}$[a] (nm)	$\lambda_{em,max}$[b] (nm)	ε[c] (M^{-1} cm^{-1})	Additional information	Manufacturer
DY-350 (DyLight 350)	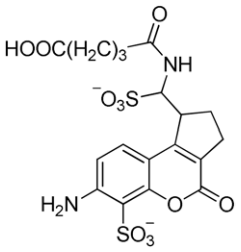	353	432	19 000 (15 000)	in PBS	Dyomics GmbH (Life Technologies)
DY-360XL	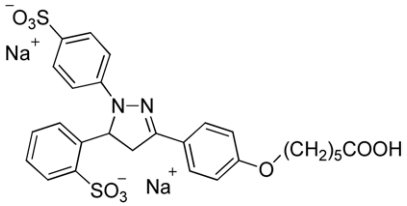	362	459	25 000	in PBS; STED: 592 nm (gated CW; LEICA)[f] or 595 nm (pulsed; Abberior)[f]	Dyomics GmbH
DY-370XL	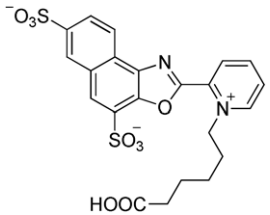	368	473	13 200	in PBS; STED: 592 nm (gated CW; LEICA)[f] or 595 nm (pulsed; Abberior)[f]	Dyomics GmbH
DANSYL (chloride)	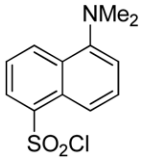	370–410 ($ArSO_2N$)	490–510 ($ArSO_2N$)	3300–4500	The reagent is nonfluorescent; it reacts with amines and forms fluorescent sulfonamides ($ArSO_2N$)	Life Technologies
DY-375XL	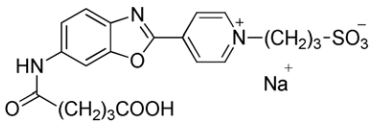	376	543	16 000	in EtOH; STED: 660 nm (gated CW; LEICA)[f]	Dyomics GmbH

(***Continued***)

Table 1. (*Continued*)

Name	Structure	$\lambda_{abs,max}$ [a] (nm)	$\lambda_{em,max}$ [b] (nm)	ε [c] (M^{-1} cm^{-1})	Additional information	Manufacturer
DY-380XL	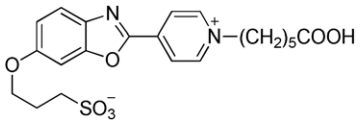	381	510	22 000	in EtOH; STED: 592 nm (gated CW; LEICA)[f] or 595 nm (pulsed; Abberior)[f]	Dyomics GmbH
VioGreen	—	388	520	—	STED: 592/595 nm (LEICA / Abberior) or 660 nm (LEICA)[f] ?	Miltenyi Biotec
Atto 390	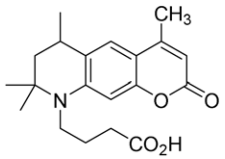	390	479	24 000	$\Phi_{fl} = 0.90$, $\tau_{fl} = 5.0$ ns in H_2O; STED: 592/595 nm (LEICA / Abberior)[f]	Atto-Tec GmbH
Dapoxyl carboxylic acid, succinimidyl ester	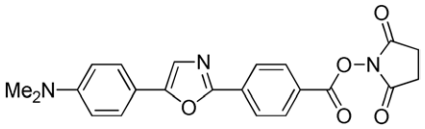	395	600	23 500	in MeOH (solvatochromic) STED: 765/775 nm (Picoquant/Abberior/ LEICA)[f]	Life Technologies
DY-395XL	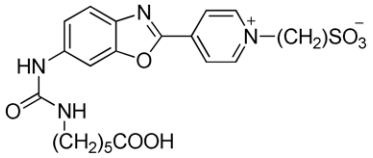	396	572	20 000	in EtOH, STED: 765/775 nm (Picoquant/Abberior/LEICA)[f]	Dyomics GmbH
Krome Orange	—	398	528	17 665	in H_2O, STED: 592/595 nm (LEICA / Abberior) or 660 nm (LEICA)[f] ?	Beckman Coulter
Pacific Blue	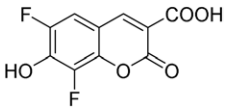	400	447	29 500	$\Phi_{fl} = 0.55$ in H_2O; STED: 592/595 nm (LEICA / Abberior)[f] ?	Life Technologies
Pacific Orange	—	400	551	—	in H_2O; STED: 660 nm (LEICA)[f]	Life Technologies
SeTau-405	—	405 (391)	518 (498)	13 800 (15 000)	$\Phi_{fl} = 0.51$ (0.32), $\tau_{fl} = 9.0$ (8.5) ns in H_2O (ethanol)	SETA BioMedicals
Pacific Green	—	410	500	—	in H_2O	Life Technologies

(***Continued***)

Table 1. (*Continued*)

Name	Structure	$\lambda_{abs,max}$ [a] (nm)	$\lambda_{em,max}$ [b] (nm)	ε [c] (M^{-1} cm^{-1})	Additional information	Manufacturer
V500	—	415	500	—	STED: 592/595 nm (LEICA / Abberior)[f]	BD Biosciences
PyMPO, succinimidyl ester	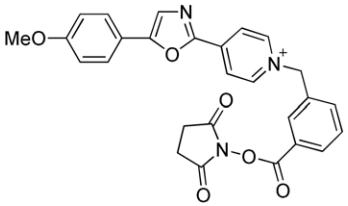	415	570	26 000	in MeOH (emission shifts to shorter wavelengths in nonpolar solvents)	Life Technologies
APTS	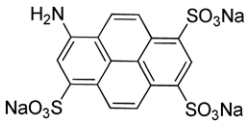	424	505	20 000	in H_2O; STED: 592/595 nm (LEICA / Abberior)[f]	Sigma-Aldrich
Atto 425	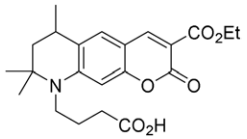	436	484	45 000	$\Phi_{fl} = 0.65$, $\tau_{fl} = 4.0$ ns in aqueous PBS	Atto Tec GmbH
Lucifer Yellow CH: 'an angel rather than the devil'	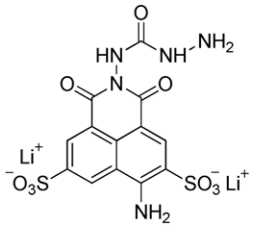	428	540	11 500	in H_2O; STED: 660 nm (LEICA)[f]	Life Technologies
Alexa Fluor 430	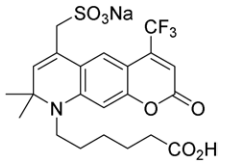	431	541	16 000	$\Phi_{fl} = 0.55$ in H_2O; STED: 660 nm (LEICA)[f]	Life Technologies

(***Continued***)

Table 1. (*Continued*)

Name	Structure	$\lambda_{abs,max}$[a] (nm)	$\lambda_{em,max}$[b] (nm)	ε[c] (M^{-1} cm^{-1})	Additional information	Manufacturer
Atto 430LS	—	433	547	32 000	$\Phi_{fl} = 0.65$, $\tau_{fl} = 4.0$ ns in PBS; STED: 660 nm (LEICA)[f]	Atto-Tec GmbH
Star 440 SXP	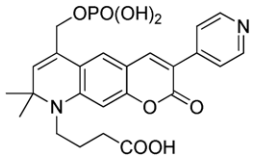	436	515	22 700	$\Phi_{fl} = 0.68$, $\tau_{fl} = 3.3$ ns in PBS; STED: 592/595 nm (LEICA / Abberior)[f]	Abberior GmbH
DY-431	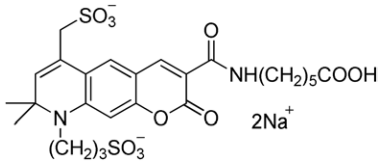	442	496	35 000	in PBS; STED: 592/595 nm (LEICA / Abberior)[f]	Dyomics GmbH
Atto 465	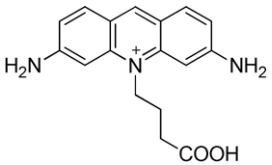	453	508	75 000	$\Phi_{fl} = 0.75$, $\tau_{fl} = 5.0$ ns in H_2O; STED: 592/595 nm (LEICA / Abberior) or 660 nm (LEICA)[f] ?	Atto-Tec GmbH
Pulsar 650	Ruthenium complex	458	647		in phosphate buffer at pH 7, STED: 765/775 nm (Picoquant/Abberior/ LEICA)[f]	Biosearch Technologies
NBD-X, succinimidyl ester	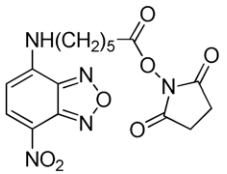	466	534	22 000	in MeOH	Life Technologies

(***Continued***)

Table 1. (*Continued*)

Name	Structure	$\lambda_{abs,max}$[a] (nm)	$\lambda_{em,max}$[b] (nm)	ε[c] (M^{-1} cm^{-1})	Additional information	Manufacturer
Star 470 SXP	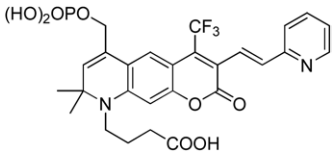	472	624	29 000	$\Phi_{fl} = 0.12$, $\tau_{fl} = 0.8$ ns in PBS; STED: 765/775 nm (Picoquant/Aberior/LEICA)[f]	Abberior GmbH
DY-485XL (DyLight 485-LS)	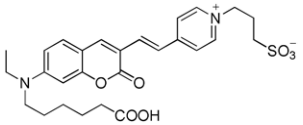	482	560	48 000	in H_2O; STED: 660 nm (LEICA)[f]	Dyomics GmbH (Life Technologies)
DY-510XL (DyLight 510-LS)	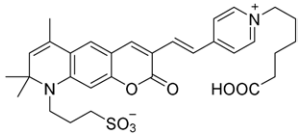	493 (509)	585 (590)	40 000 (50 000)	in H_2O (ethanol); STED: 660 nm (LEICA)[f] ?	Dyomics (Life Technologies)
Propidium iodide	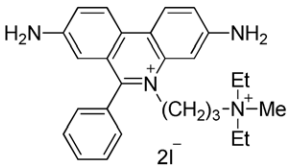	493, 535 (bound)	635, 617 (bound)	6000	in phosphate buffer (pH 7); STED: 765/775 nm (Picoquant/Abberior/LEICA)[f]	Life Technologies
Chromeo 494	—	494	628	55 000	in PBS; STED: 765/775 nm (Picoquant/Abberior/LEICA)[f]	Active Motif
Atto 490LS	—	496	661	40 000	$\Phi_{fl} = 0.30$, $\tau_{fl} = 2.6$ ns in PBS; STED: 765/775 nm (Picoquant/Abberior/LEICA)[f]	Atto-Tec GmbH
DY-480XL	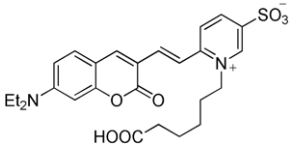	500	630	50 000	in EtOH; STED: 765/775 nm (Picoquant/Abberior/LEICA)[f]	Dyomics GmbH

(***Continued***)

Table 1. (*Continued*)

Name	Structure	$\lambda_{abs,max}$ [a] (nm)	$\lambda_{em,max}$ [b] (nm)	ε [c] (M^{-1} cm^{-1})	Additional information	Manufacturer
DY-511XL	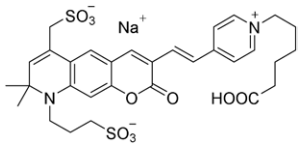	510	595	47 000	in EtOH; STED: 660 nm (LEICA)[f] ?	Dyomics GmbH
DY-481XL (DyLight 515-LS)	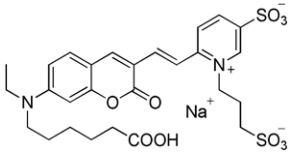	515	650	50 000	in EtOH; STED: 765/775 nm (Picoquant/Abberior/LEICA)[f]	Dyomics (Life Technologies)
DY-520XL	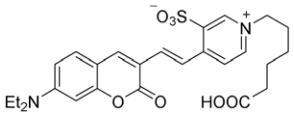	520	664	50 000	τ_{fl} = 2.6 ns in EtOH; STED: 765/775 nm (Picoquant/Abberior/LEICA)[f]	Dyomics GmbH
STAR 520 SXP	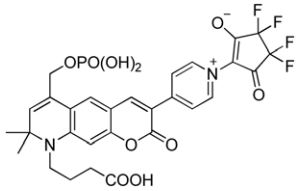	522	632	42 500	STED: 765/775 nm (Picoquant/Abberior/LEICA)[f]	Abberior GmbH
DY-521XL (DyLight 521-LS)	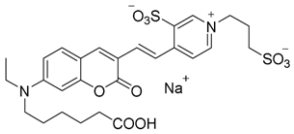	523	668	50 000	in EtOH; STED: 765/775 nm (Picoquant/Abberior/LEICA)[f]	Dyomics GmbH (Life Technologies)
Nile Red	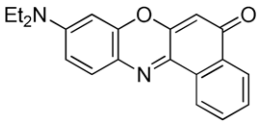	552	636	43 000	in MeOH; STED: 765/775 nm (Picoquant/Abberior/LEICA)[f]	Life Technologies

(***Continued***)

Table 1. (*Continued*)

Name	Structure	$\lambda_{abs,max}$[a] (nm)	$\lambda_{em,max}$[b] (nm)	ε[c] (M^{-1} cm^{-1})	Additional information	Manufacturer
LUB04 [83]	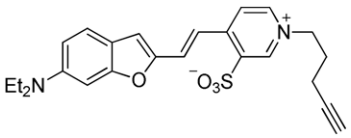	588	744	28 000	in aq. PBS; for the copper catalyzed 'click-chemistry'	Luminochem Sigma-Aldrich
DY-601XL	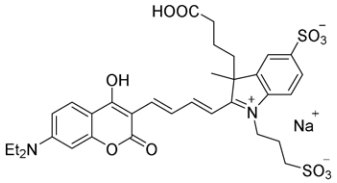	606	663	85 000	in EtOH; STED: 765/775 nm (Picoquant/Abberior/LEICA)[f]	Dyomics GmbH

[a] Absorption maximum.
[b] Fluorescence emission maximum.
[c] Molar extinction coefficient.
[d] In the presence of 10 mM CaEGTA.
[e] In the presence of 100 mM KCl, 10 mM MOPS, pH 7.20.
[f] Abberior Instruments GmbH offers STED microscopes with pulsed 595 nm and 775 nm lasers; LEICA Microsystems—with 592 nm (gated; CW), 660 nm (gated; CW) and 775 nm (pulsed) lasers; Picoquant GmbH offers a STED microscope with pulsed 765 nm depletion laser.

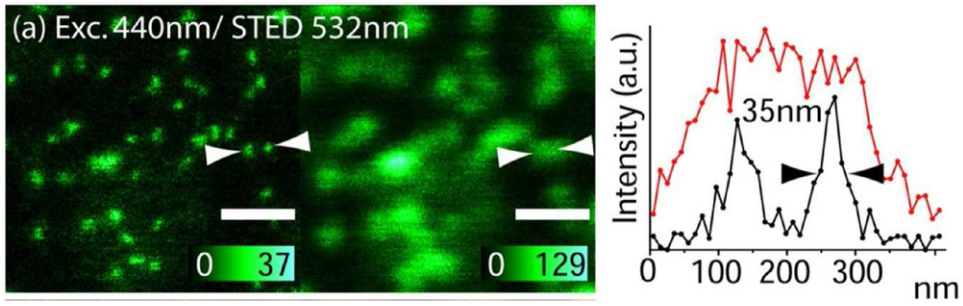

Figure 4. Left, STED and confocal images of 20–30 nm silica beads labeled with ATTO 425 (for structure, see table 1), scale bars = 500 nm; right, line-profile measurements, at sites indicated by arrows [98].

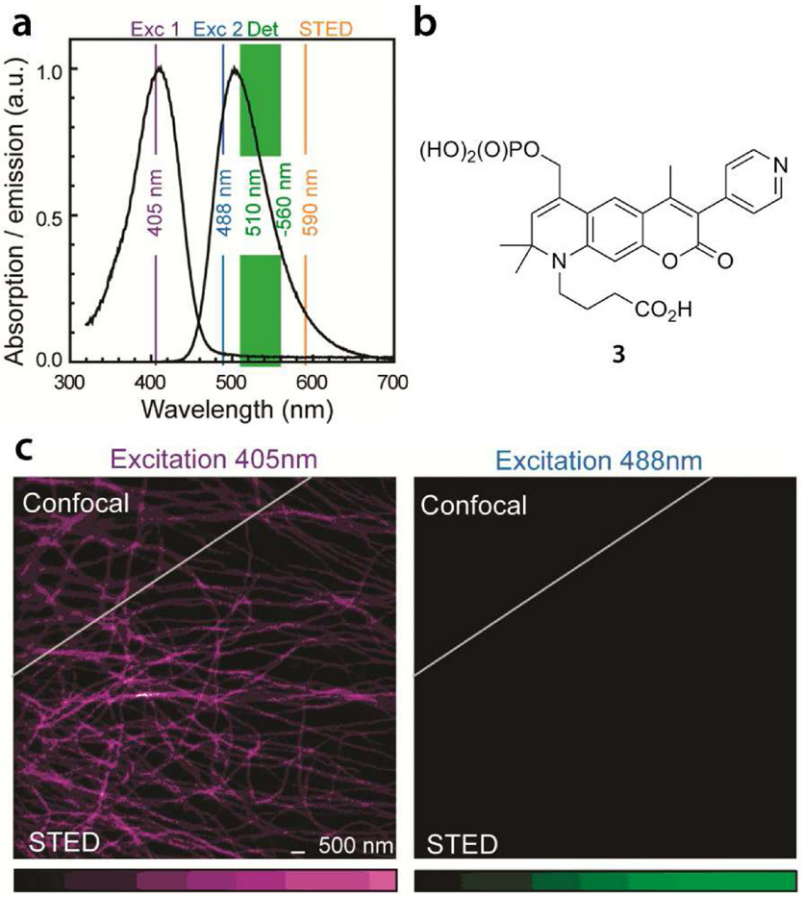

Figure 5. Confocal and STED microscopy imaging without noticeable cross-talk. (a) Absorption and emission spectra of compound **3**. The violet 405 nm laser line is almost in the absorption maximum whereas the 'standard' 488 nm light cannot excite compound **3**. (b) Chemical structure of compound **3**. (c) Microtubules visualized through immunolabeling with compound **3** were irradiated with 405 and 488 nm lasers in an alternating manner with an emission cross-talk less than 1%; images were recorded in confocal and STED modes. Reproduced with permission from [90].

dimethyl- or diethylamino groups. Therefore, they are directly conjugated with an electron-acceptor part of the coumarin fluorophore, and the fully developed 'push–pull' effect shifts the absorption and emission bands further to longer wavelengths.

Fluorescent dyes with large Stokes shifts and their use in STED microscopy

The far-red STED wavelength of 775 nm emerged at the very beginning of STED microscopy, and was present in the first commercial STED microscope (2007, LEICA Microsystems). Three STED wavelengths currently available in commercial STED microscopes are: 592−595 nm, 660 nm and 765−775 nm. Leica Microsystems offers STED microscopes with 592 nm (gated; CW), 660 nm (gated; CW) and 775 nm (pulsed) STED lasers. Abberior Instruments GmbH produces STED microscopes with 595 nm (pulsed) and 775 nm (pulsed) STED lasers. PicoQuant GmbH offers a STED microscope with a 765 nm STED laser. The imaging results reviewed below were often obtained in non-commercial setups, using various depletion wavelengths in the green–orange and

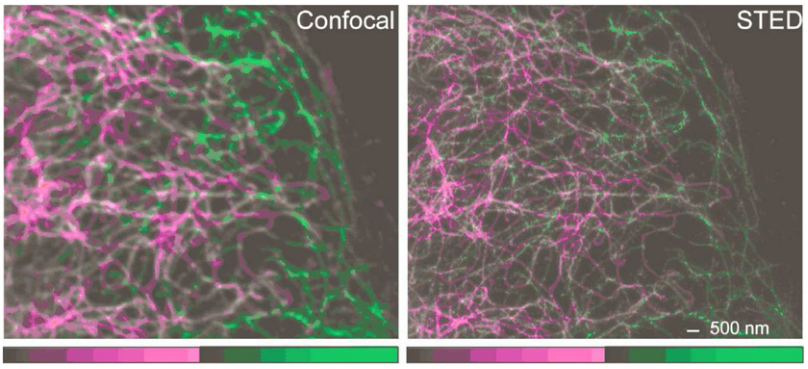

Figure 6. Confocal and STED microscopy images of vimentin (magenta) and microtubule (green), two components of the cytoskeleton in a fixed mammalian PtK2 (Potorous tridactylus, kidney) cell. Vimentin was immunolabeled with NHS ester Abberior Star 440 SXP dye (for structure, see table 1); excitation with 405 nm. Tubulin was immunolabeled with Oregon Green™ 488; excitation with 488 nm. The excitation of both dyes was alternated line-by-line to separate the fluorescence in time. Detection at 510 – 560 nm for both dyes; STED at 590 nm for both dyes (STED power 84 mW at the back focal plane) (Reproduced with permission from [90]).

red spectral regions. However, for most of the dyes mentioned in this review, the first super-resolution imaging experiments realized with 'non-classical' STED lasers can probably be reproduced (and their results even improved) by using three 'modern' STED regimes: 592–595 nm, 660 nm and 765–775 nm. Indeed, most of the fluorescent dyes (and especially dyes possessing large Stokes shifts) have broad absorption and emission bands. This feature enables to use a very sparsely populated set of STED wavelengths, and optimize the STED power rather than the STED wavelength. Remarkably, the common and most important STED wavelength region all manufactures offer in their STED microscopes belongs to a far-red spectral range of 765–775 nm (not visible by the bare eye). Red light is non-invasive, possesses greater tissue penetration depth, reduced scattering, and does not cause protein auto-fluorescence. Additionally, the red shift of the emission and absorption bands can expand the spectral window for dual- and multicolor STED imaging experiments which utilize two or more dyes. (It may even require shifting the STED wavelength further to the red spectral region). The appropriate wavelengths for the excitation of the 'stedable' fluorescent dyes include 488 nm (for dyes with large Stokes shifts), green 532 nm and 552 nm lasers, as well as red 640 nm laser (for excitation of the red-emitting dyes undergoing STED at 775 nm). Unlike STED lasers, various excitation sources are easily available, and it is possible to 'tune' the wavelength of the excitation light and bring it to the required position.

Surprisingly, there are not so many examples of the studies in which a large Stokes shift dye (or its combination with a 'normal' dye) was used as a fluorescent label in optical super-resolution microscopy. This may be due to the lower photostability and brightness (product of the fluorescence quantum yield and extinction coefficient) of the most dyes with large Stokes shift. However, there are modern bright and photostable large Stokes shift dyes, and they were successfully applied in optical 'nanoscopy'.

However, at the beginning, it was not clear if STED microscopy is applicable to dyes with large Stokes shifts. Initially, only most photostable xanthenes (rhodamines) or carbopyronines were shown to perform well under STED conditions and provide super-resolution (these dyes possess small Stokes shifts). Interestingly, the first realization of the two-color STED microscopy involved two dyes (rhodamine and carbopyronine) with small Stokes shifts and, as a consequence, two excitation and two STED lasers [97]. All dyes with large Stokes shifts (see table 1) are intrinsically less photostable than rhodamines and carbopyronines. They bleach faster, especially when exposed to very powerful STED light. Therefore, they withstand less number of STED pulses, and afford lower optical resolution than xanthene dyes, carbopyronines, newly emerged silicon-rhodamines or other photostable fluorochromes with small Stokes shifts.

However, initial studies demonstrated that coumarin dyes (e.g. ATTO 425; see table 1) can indeed be applied in STED microscopy. As a proof of another principle, the suitability of light from a multicolor, stimulated Raman scattering (SRS) source for gaining STED resolution was successfully demonstrated using silica beads. The SRS light source consists of a microchip laser coupled to a fiber where the SRS occurs. The beads were labeled with a commercially available coumarin dye ATTO 425 and imaged in a custom-built STED microscope (figure 4) [98]. Unlike the supercontinuum light source used in another STED microscope [99], the optical power of the SRS light source is preserved within narrow peaks in a comb-like spectrum, the output light is linearly polarized, and light suitable for STED is produced below 630 nm. Thus, for ATTO 425 dye, STED was performed at 532 nm (the fundamental wavelength from the comb spectrum of the SRS light source). In this case, excitation of the fluorophore was accomplished using a 440 nm diode laser. Due to simplicity, compactness, broad spectral output and low cost, SRS sources could become an attractive option for spectrally flexible STED imaging.

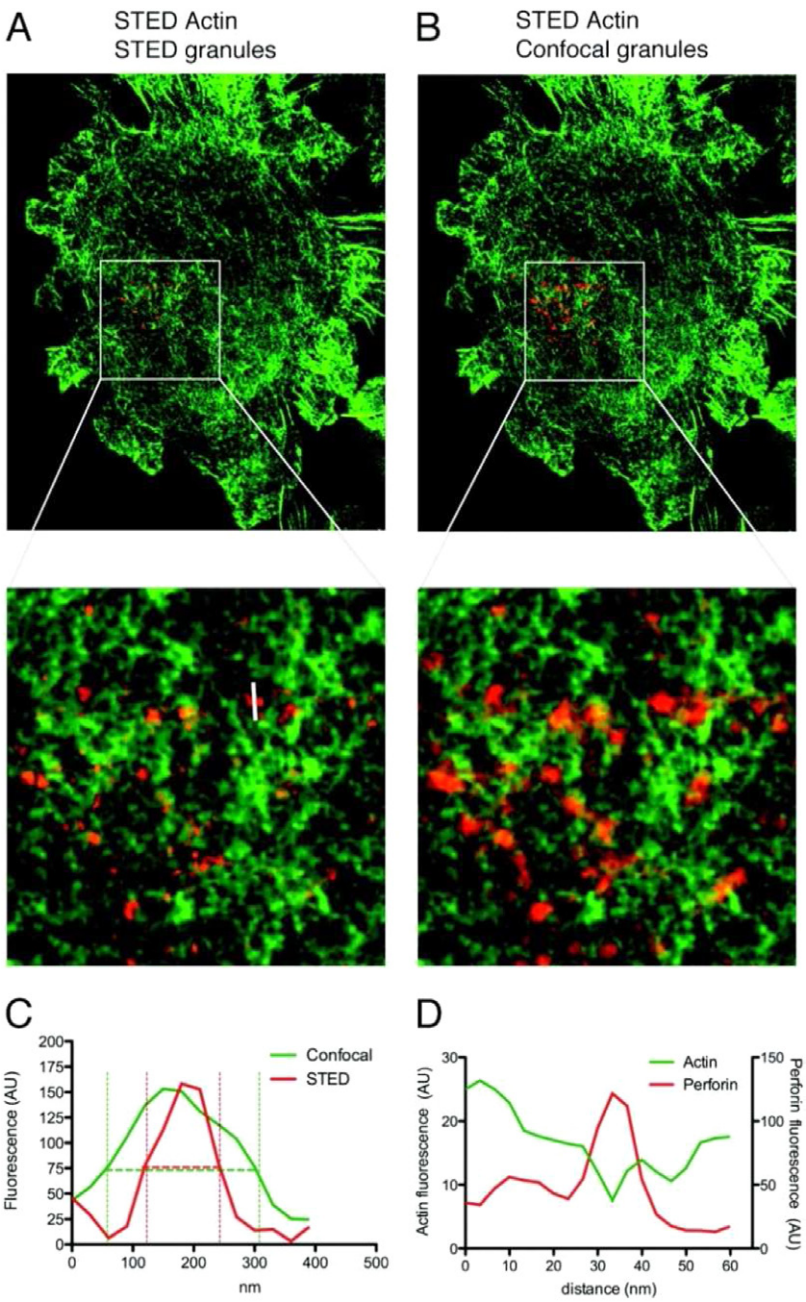

Figure 7. Visualization of lytic granules imaged by CW-STED and confocal on F-actin [101]. Fixed cells were imaged using CW-STED (actin stained with Alexa Fluor 488, green) and either CW-STED or confocal (perforin stained with Pacific Orange™, red). Shown is the same cell with granules detected by STED (A) or confocal (B). A region of interest is enlarged to show greater resolution of granules (center panel). (C) Full width half maximum (FWHM) measurements of confocal (green line) and STED images (red line). Horizontal dashed lines show half maxima, vertical dashed lines show width at half maxima. (D) Representative line profile of pixel intensities of actin (green line) and perforin (red line) taken from a line bisecting a single granule (shown in white in STED image enlargement).

The applicability of the dual-color STED microscopy in material science was demonstrated in another publication, in which localization and repartition of fluorescent polymer nanoparticles of about 100 nm size was studied in nanofibers [100]. As a rule, the BODIPY dyes are difficult to use in STED microscopy, because they have small Stokes shifts and their fluorescence can easily be re-excited by the very powerful STED beam. However, a hydrophobic and polymerizable BODIPY dye B504-MA found to be applicable in STED nanoscopy. It was used to label the polymer nanoparticles, whereas the PVA matrix was stained with a water-soluble derivative of perylenetetracarboxylic acid (PTCA) with a comparatively large Stokes shift. This combination of fluorophores allowed using the excitation with different lines of the same argon laser (458 nm for PTCA and 514 nm for B504-MA). The emission spectra of these fluorophores overlap considerably. Therefore, efficient depletion using a single STED beam at 592 nm could be achieved. The nanoparticle sizes and nanofiber thicknesses were shown to be in good agreement with the values obtained by electron microscopy.

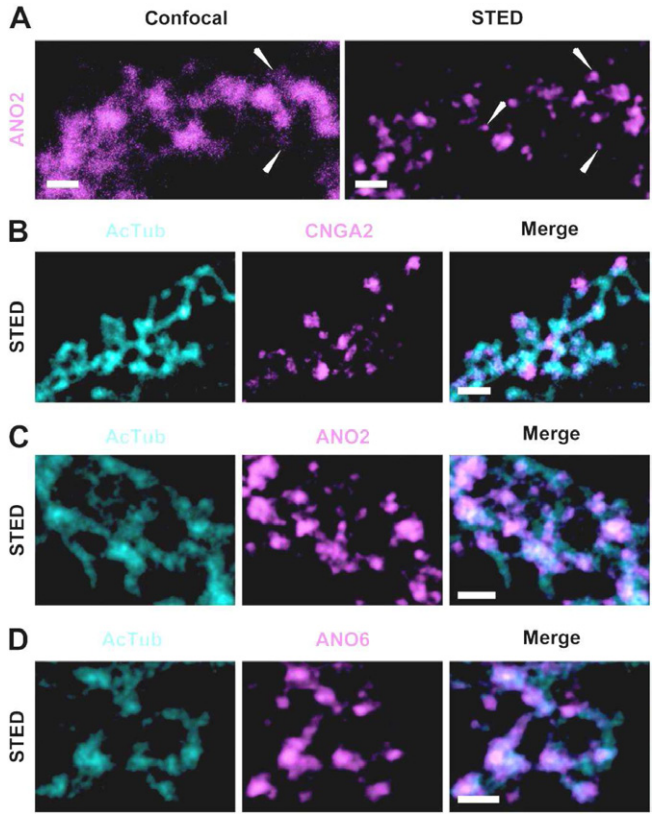

Figure 8. Clustered localization of CNGA2 and anoctamins in olfactory cilia (Reproduced with permission from [102]). (A) Frontal sections of olfactory epithelium were stained for ANO2 and analyzed with conventional confocal and STED microscopy, demonstrating the increase in resolution when switching to the STED mode. Single clusters that were not visible in the confocal picture (examples are indicated by arrowheads) can clearly be seen in the STED images. Co-localization of (B) CNGA2, (C) ANO2 and (D) ANO6 (magenta) and acetylated tubulin (cyan), showing clusters stained by the different antibodies. Scale bars = 500 nm.

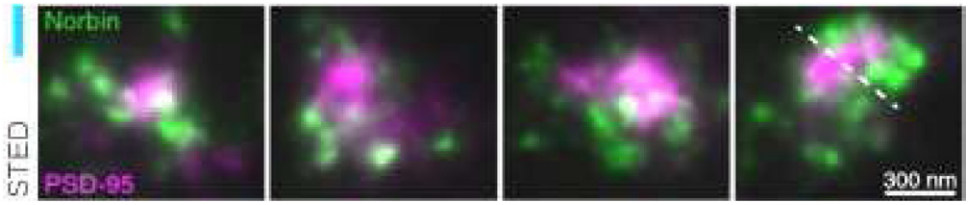

Figure 9. Dual color STED reveals that Norbin (green) does not colocalize with PSD-95 (magenta). Scale bar 300 nm [103].

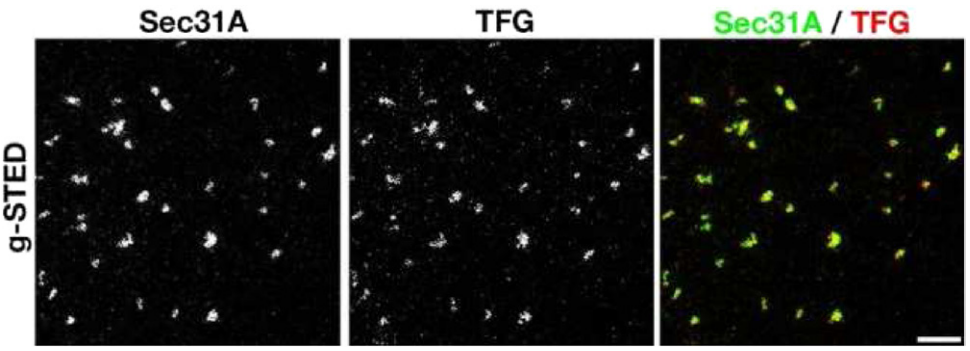

Figure 10. The distributions of endogenous TFG (shown red in the right picture) and Sec31A (a subunit of COPII, shown green in the right picture) were examined using gated STED (gSTED) (Reproduced with permission from [104]). Scale bar = 1 μm.

An obvious generalization of this approach would be always to combine two dyes—one with a large Stokes shift and one with a small Stokes shift—and switch-off the fluorescence of both of them using one STED laser (figure 5). The most straightforward implementation includes a pair of dyes, both of which

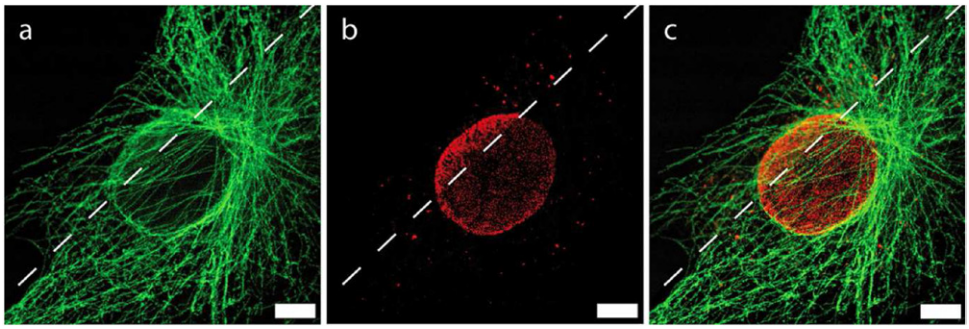

Figure 11. Ptk-2-cell in which microtubules are labeled by Alexa 488 (section (*a*), green) and the component of the nuclear pore complex NUP153 by Abberior 440 SXP (section (*b*), red) [106]. Color overlay of the respective images (section (*c*)). Scale bars = 5 μm.

can be depleted with 'green–orange' STED lasers (592 or 595 nm).

Photostable 'blue' dyes with large Stokes shift are rare (see table 1). On the other hand, there are plenty of photoresistant green-emitting dyes which can be excited with an argon laser (488 nm line) and depleted with 592/595 nm STED lasers (for example, Alexa Fluor 488, ATTO 488, Abberior Star 488, Oregon Green, Chromeo 488, CF 488 A, and others). These dyes have small Stokes shifts and may be combined with the selected 'blue' dyes possessing relatively large Stokes shifts (figure 5), provided that there will be minimal cross-talks by excitation with two lasers. This means that in an ideal case the 405 nm laser diode excites only the fluorescence of the 'blue' dye, and 488 nm line of argon laser—the fluorescence of the 'green' dye. The cross-talk is a crucial parameter, because 'green' dyes are represented in most cases by xanthenes with high absorption coefficients, and these are also sensitive to UV-excitation. On the other hand, when used with Oregon Green dye, the large Stokes shift marker Abberior Star 440 SXP (figure 6) shows a crosstalk of 19% when excited with 488 nm. Nevertheless, due to their large Stokes shifts and high photostability, phosphorylated coumarins (Abberior Star 440 SXP, 470 SXP and 520 SXP) enable to combine multilabel imaging (using one detector and several excitation sources) with diffraction unlimited optical resolution. They provide an optical resolution of 40–60 nm with a low background signal. In conjugates with antibodies, phosphorylated coumarins were found to display higher quantum yields than the corresponding sulfonylated coumarins (with the same fluorophore) [90].

The following examples are also based on the use of 592/595 nm STED light and illustrate the advantages of this approach in more detail. Mace *et al* [101] used dual-color CW-STED microscopy and revealed that in natural killer cells NK92, lytic granules (specialized lysosomes secreted by NK cells for the elimination of diseased and tumorigenic targets) are closely associated with F-actin and thus secreted through minimally sized clearances (figure 7). For imaging, NK cells were fixed, permeabilized and stained for F-actin using (amino) phalloidin bearing Alexa Fluor 488 dye. The lytic granule component perforin was labeled with a large Stokes shift dye Pacific Orange™ which was conjugated to the anti-perforin antibody.

Dual-color STED microscopy provided morphological evidence for the organization of anoctamins (voltage sensitive calcium-activated chloride channels) and cyclic nucleotide gated (CNG) channels in distinct domain, thus indicating the existence of signaling microdomains in cilia of olfactory sensory neuron (OSN) [102]. In addition, the staining patterns for anoctamins ANO2 and ANO6 observed in high-resolved STED images supported the idea that ANO2 and ANO6 form oligomeric complexes in olfactory cilia (figure 8). Large Stokes shift dye V500 (BD Horizon) was used for staining tubulin, whereas anoctamins and CNG channels were immunochemically stained with Oregon Green 488—a conventional dye with a small Stokes shift. Images were acquired using two excitation sources at 458 nm (for V500) and 514 nm (for Oregon Green 488) and one STED laser (592 nm). V500 and Oregon Green 488 emission was detected at 465−500 and 540−585 nm, respectively. Unfortunately, V500 dye (BD Horizon) is available only in bioconjugates. No active esters or other derivatives of this marker with reactive groups (maleimides, azides, alkynes, etc) are commercially available. The structures of Pacific Orange and V500 dyes are unknown.

Large Stokes shift dyes Abberior Star 440 SXP and Abberior Star 520 SXP (Abberior GmbH) were utilized in colocalization studies on Norbin (neuron-specific cytosolic protein which interacts with the metabotropic glutamate receptor) and postsynaptic density protein 95 (PSD-95) in neurons [103]. Neuron spines have a submicrometer size, and therefore all constituting proteins appear as more or less colocalized in a confocal microscope. Using super-resolution microscopy methods—3D-SIM and STED, authors showed that Norbin associates with actin rather than with PSD-95 in dendritic spines (figure 9).

Using multiple super-resolution imaging techniques, including two-color gated STED (gSTED) microscopy, which provided spatial resolution down to ~50 nm, Johnson *et al* [104] found that endogeneous TFG protein tightly colocalized (see figure 10) with

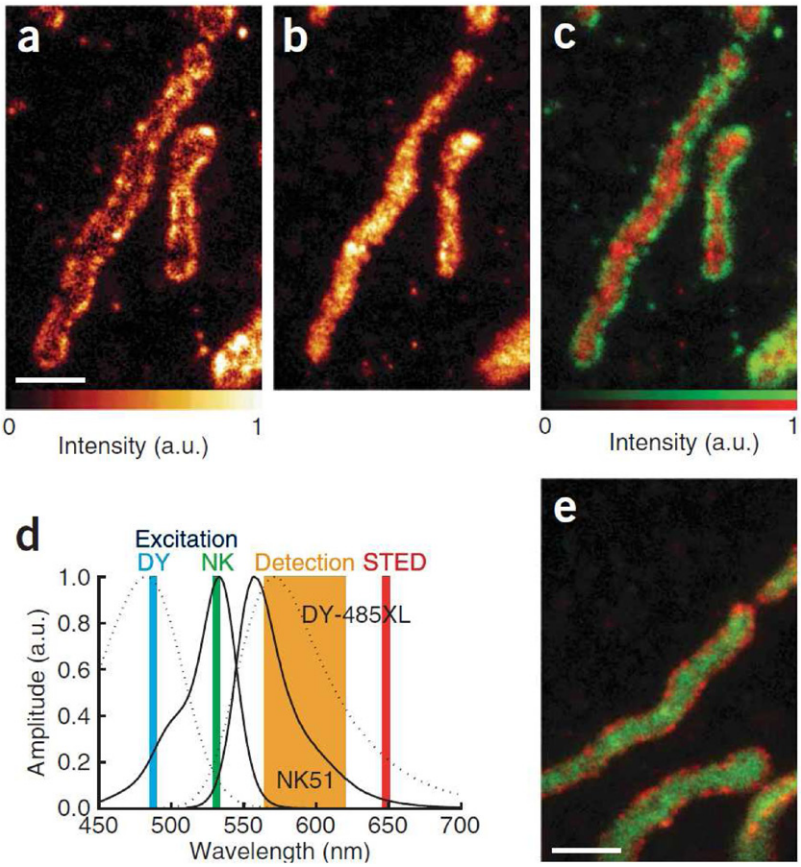

Figure 12. Two-color isoSTED imaging of mitochondria in Vero cells [110]. (a), (b) Distribution of the outer membrane protein Tom20 labeled with the organic fluorophore DY-485XL (a) and of the NK51-labeled matrix protein mtHsp70 (b). (c) Overlay of the two images showing Tom20 in green and mtHsp70 in red. (d) Excitation and absorption spectra for DY-485XL (dotted line) and NK51 (solid line). The two fluorophores are separated by subsequently exciting the sample at 488 nm (DY-485XL) and 532 nm (NK51). Both dyes are depleted by stimulated emission at 647 nm. (e) Reverse staining as a control (Tom20 with NK51 and Hsp70 with DY-485XL) yields similar results as the initial recording (c). Scale bars = 1 μm.

both inner and outer subunits of COPII (protein coating a vesicle which transports proteins from the rough endoplasmatic reticulum to the Golgi apparatus). For immunochemical staining, large Stokes shift dye Abberior Star 440 SXP was used together with small Stokes shift dyes DyLight 488 and Alexa Fluor 488, 568 and 647. Imaging was performed using commercial Leica TCS STED system. According to recommendations of LEICA Microsystems, Abberior Star 440 SXP is a viable substitute for V500 dye (BD Horizon) [105].

Another example of dual-color STED imaging was obtained when microtubules and the nuclear pore complex component NUP153 of Ptk-2-cells were labeled by Alexa 488 and the large Stokes shift dye Abberior Star 440 SXP, respectively (figure 11) [106]. For excitation of these dyes, laser sources at 470 nm and 488 nm, respectively, were utilized, whereas a single STED laser at 592 nm was used for the depletion. Fluorescence detection was realized at 480−500 nm (for Alexa Fluor 488) and 510 −560 nm (for Abberior Star 440 SXP). Other applications of the large Stokes shift dye Abberior Star 440 SXP in super-resolution microscopy were reported the following studies [107–109].

Another (gated, CW) STED wavelength of 660 nm is available in the commercial light microscope produced by LEICA Microsystems. The results reported in 2008 can help to choose the proper pairs of fluorescent dyes (with large and small Stokes shifts) which could be depleted using 660 nm light [110]. In this report, the commercially available coumarin dye DY-485XL was used together with the small Stokes shift rhodamine dye NK51 to demonstrate the advantages and illustrate the principles of isoSTED (a combination of STED and 4Pi[1] microscopies to improve resolution along *Z*-axis). Two-color isoSTED enables imaging of the spatial distribution of two or more (biological) objects at the nanoscale in 3D [110]. In particular, the method of isoSTED strongly improves the resolution in *z*-direction: instead of being about 500–600 nm as in confocal microscopy, it becomes 30–50 nm (depending on the STED power, dye and sample properties). In other words, isoSTED enables uniform optical resolution in all 3D. The coumarin dye DY-485XL (for structure, see table 1) displays a similar emission spectrum as rhodamine dye NK51, whereas its excitation spectrum is blue-shifted by ~50 nm (figure 12). This

[1] 4Pi-microscope is a variation of confocal microscope, in which the improvement in axial resolution is achieved by using two opposing lenses focusing light to the same location.

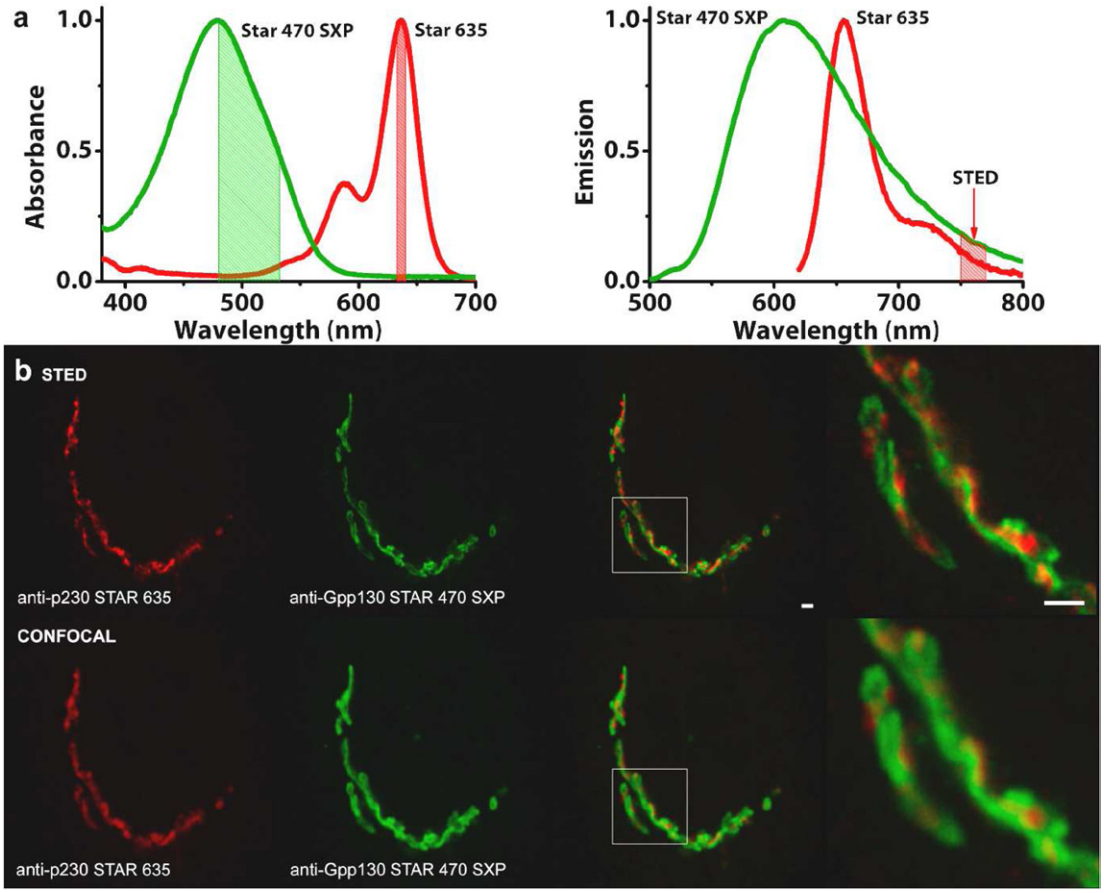

Figure 13. (a) Normalized absorption (left) and emission (right) spectra of Abberior STAR 470 SXP (green line) and Abberior STAR 635 (red line) attached to antibodies in aqueous PBS buffer at pH 7.4. (b) Two-color STED (upper panel) and confocal (lower panel) images of the Golgi apparatus. HeLa cells were fixed and probed with primary antibodies against Gpp130 and p230 to stain the *trans*- and *cis*-sides of the Golgi ribbon, respectively. Secondary antibodies conjugated with Star 470 SXP and Star 635 dyes were then applied. Two-color STED images were acquired using a commercial Leica TCS STED microscope (Reproduced with permission from [91]). Scale bars = 1 μm.

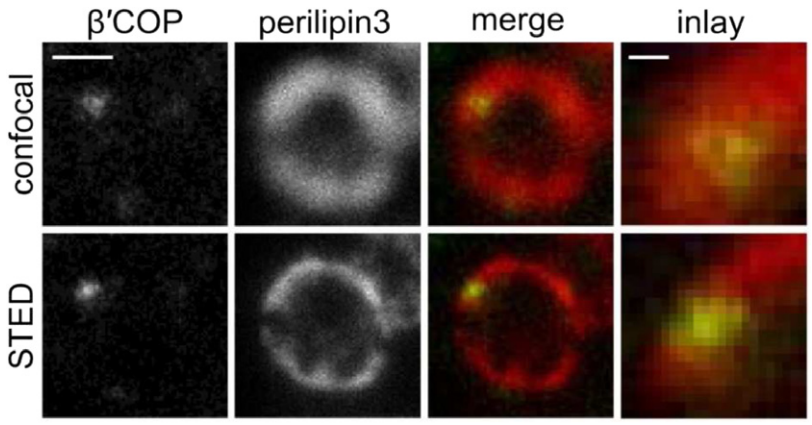

Figure 14. Localization of β'COP (green) to the LD surface (perilipin3, red) using confocal (upper panel) and super-resolution STED microscopy (lower panel) [113]. Scale bars = 500 nm (overview) or 100 nm (inlay).

combination of fluorophores allowed using only one STED beam at 647 nm and two readily available excitation lasers with emission at 488 nm (for DY-485XL) and 532 nm (for NK51). In this study, mitochondrial outer membrane protein Tom20 was labeled by indirect immunostaining with coumarin DY-485XL (Dyomics GmbH), and the matrix protein mtHsp70—with rhodamine dye NK51. The images were recorded by subsequent excitation of the sample at 488 nm (channel 1) and 532 nm (channel 2) and depletion of the fluorescence by stimulated emission triggered by 647 nm laser. As it can be seen from figure 12, rhodamine NK51 is excited also with 488 nm light, and the residual excitation cross-talk between two channels

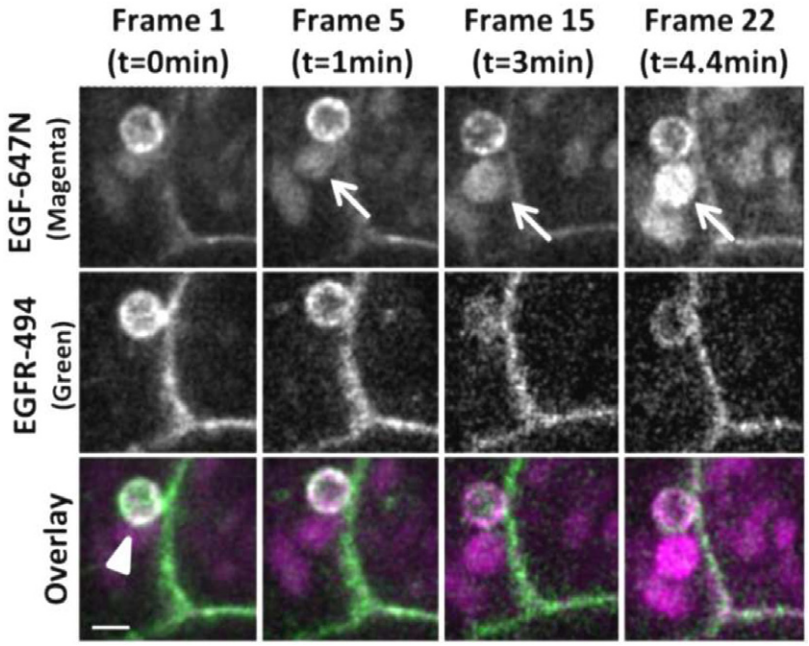

Figure 15. A time series of 2-color STED images (raw data) of living cells (HEK293) labeled with EGF-CLIP$_f$-ATTO647N (magenta) and EGFR-SNAP$_f$-Chromeo494 (green) Reproduced with permission from ([115]). Scale bars = 1 μm.

had to be removed by linear unmixing applied to the raw data. As a result, two proteins of an organelle inside the whole cell were imaged separately with nanoscale 3D resolution in the 50 nm range. These dual-color images demonstrated for the first time the possibilities and difficulties (cross-talk, uneven photobleaching) of two-color STED microscopy.

This successful combination of dyes (coumarin DY-485XL and a derivative of Rhodamine 6G with large and small Stokes shifts, respectively) reported in 2008 [110] prompted to use the same fluorophores in another study published in 2012 [111]. Owing to enhanced optical resolution, STED microscopy allows to resolve single vesicles in cells. Using dual color STED, Dean *et al* [111] found that after 15 min treatment of neurons with glycine (to induce neural activity), a vesicular transport protein synaptotagmin IV (syt-IV) was present on vesicles at synapses which are distinct from synaptic vesicles. At the same time, synaptotagmin I (syt-I) was shown to be localized to synaptic vesicles. For these experiments, syt-IV or syt-I were labeled with commercially available ATTO565 dye (spectral and structural analog of NK51), while synaptophysin (a protein ubiquitous in synaptic vesicles) was stained with a large Stokes shift dye DY-485XL. Excitation of ATTO565 was achieved with a diode laser at 532 nm, while DY-485XL was excited by the 470 nm line from a laser diode source. STED beam at 647 nm was used to deplete the fluorescence of both dyes. Most probably, 660 nm STED light can also be used for efficient depletion in this case. Fluorescence detection for both dyes was realized in the window between 560 and 600 nm.

In another example, topological mapping of presynaptic proteins with nanoscale resolution at the calyx of Held[2] was realized by dual-color STED microscopy [112]. Two synaptic protein components, the vesicular glutamate transporter (VGluT1) and synapsin were indirectly labeled with ATTO565 and the large Stokes shift dye DY-485XL, respectively, using standard immunohistochemistry protocols. Excitation was performed with pulsed laser irradiation at 470 nm (for DY-485XL) and 532 nm (for ATTO565). A pulsed STED laser at 647 nm depleted the fluorescence of both fluorophores. The enhanced resolution provided by STED microscopy revealed that there are synaptic vesicles lacking synapsin, and it was impossible to demonstrate this using only conventional confocal microscopy.

However, the most common and well established conditions for STED can be achieved by using 775 nm pulsed laser which requires far-red emitting fluorescent dyes. For example, the lateral resolution provided by STED (~70 nm) was sufficient to discriminate *cis*- and *trans*-Golgi cisternae in a HeLa cell, which are typically separated by at least 200 nm. In a test experiment on two-color STED imaging, transmembrane protein GPP130, which is localized to the *cis*-Golgi network, was labeled with large Stoke shift dye Abberior Star 470 SXP (see table 1), whereas protein p230, which is found in the *trans*-Golgi network, was stained with Abberior Star 635 (figure 13) [91].

Later, in a study on the function of Arf1/COPI[3] protein machinery at cellular lipid droplets (LDs) in mam-

[2] Calyx of Held is a large synapse in the mammalian auditory central nervous system.

[3] Adenosine diphosphate ribosylation factor (Arf) and the coat protein complex that initiates the budding process on the *cis*-Golgi membrane (COPI) play an important role in vesicle trafficking.

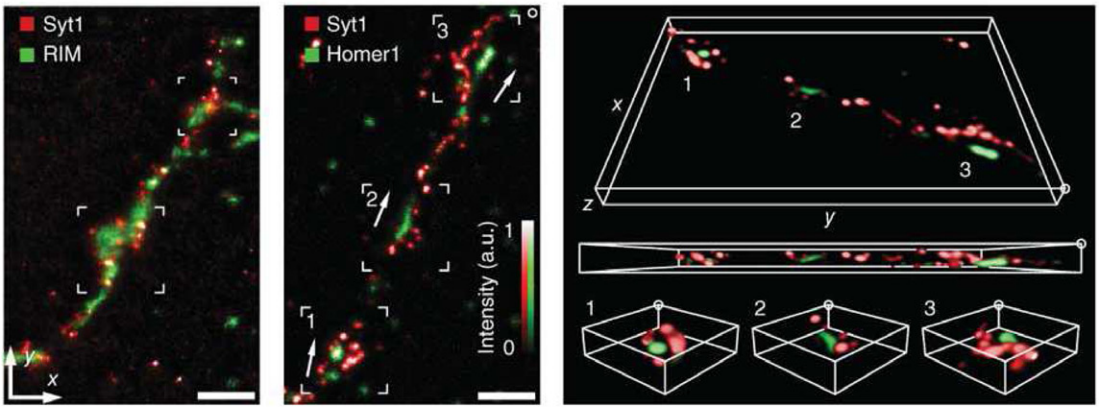

Figure 16. The localization of the surface-stranded protein Syt1 at synapses revealed by 3D dual-color isoSTED nanoscopy [119]. Syt1 was labeled with KK114 (red); postsynaptic markers RIM1, RIM2 (RIM)—with DY-480XL (green). Scale bars = 1 μm.

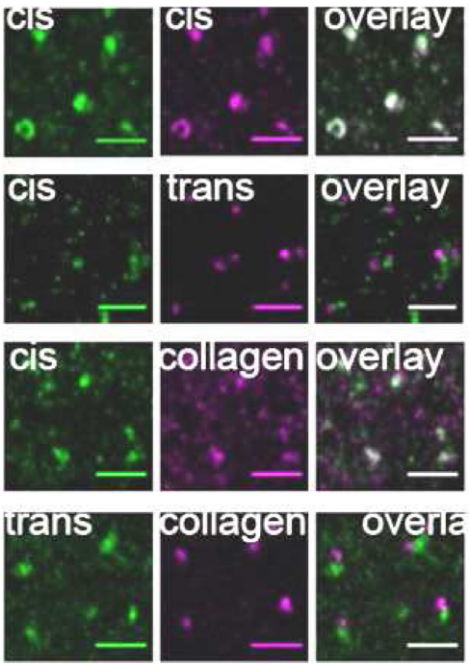

Figure 17. Two-color STED micrographs show that collagen I is retained at the *cis* face of Golgi ministacks. Reproduced with permission from ([120]). Scale bars = 2 μm.

malian NRK cells, two-color STED microscopy revealed that β' COP (a component of COPI machinery) localize to the lipid droplet surface (figure 14) [113]. For this study, β'COP and the LD marker perilipin3 were immunochemically labeled with large Stokes shift dye Abberior Star 470 SXP and conventional dye ATTO647N, respectively. Images were acquired in a custom-built microscope with a STED laser tuned to either 760 or 770 nm for the depletion. Two pulsed diode laser lasing at 510 and 640 nm were used for the excitation of Abberior Star 470 SXP and ATTO647N. Fluorescence detection was realized at 570 − 616 nm (for Abberior Star 470 SXP) and 665 − 705 nm (for ATTO647N).

In another recent report [114], two-color super-resolution STED microscopy was successfully used to assess the distribution of IQ[4] motif containing GTPase activating protein (IQGAP1) phosphorylated Rho GTPases Rac1 and Cdc42, as well as the change in their expression levels upon stimulation of *P. aeruginosa* cells with *N*-3-oxo-dodecanoyl-L-homoserine lactone (3O-C_{12}-HSL, a signaling molecule). IQGAP1 and Rac1/Cdc42 were immunochemically stained with ATTO647N and the large Stokes shift dye Abberior Star 470 SXP, respectively. Images were acquired using the commercially available Leica TCS STED microscope.

One of the brightest commercially available dyes with a large Stokes shift Chromeo™ 494[5], was used together with a carbopyronine dye ATTO647N in dual color STED microscopy in order to investigate the dynamics of the epidermal growth factor (EGF) and epidermal growth factor receptor (EGFR) proteins [115]. For this purpose, a fused protein EGFR-$SNAP_f$ was expressed in HEK293 cells and labeled with a conjugate of Chromeo™ 494 dye with aminobenzyl guanidine (BG-amine)—a small molecule recognized by the SNAP-tag. First, a conjugate of the commercially available BG-amine and a fluorescent dye was prepared. For that, BG-amine was amidated by the active ester derived from the fluorescent dye bearing a carboxyl group. In most cases, it is *N*-hydroxysuccinimidyl ester (see table 1 for structures of *N*-hydroxysuccinimidyl esters). In parallel, the $SNAP_f$-sequence (polypeptide or a 'small' protein), which is also known as a SNAP-tag, was genetically fused with the protein of interest. The SNAP-tag 'recognizes' the conjugates prepared from BG-amine with very high specificity. This 'recognition' event resulted in an efficient S_N2-reaction leading to a permanent covalent bond between the $SNAP_f$ tag and the fluorophore (via the residue of the BG-amine amidated with a fluorescent dye). This methodology enabled to obtain the EGFR-$SNAP_f$-Chromeo™ 494 conjugate. Similarly, the recombinantly expressed fused

[4] The abbreviation 'IQ' stands for the first two amino acids of the motif: isoleucine (commonly) and glutamine (invariably).
[5] Brightly fluorescent dyes with similar optical spectra—Abberior Star 470 SXP and 520 SXP—are also available (see table 1), and in many assays their immunoconjugates can be favorably compared with those prepared from Chromeo™ 494.

protein EGF-CLIP$_f$ was labeled with BC-ATTO647N, conjugate of the fluorescent dye ATTO647N with benzyl cytosine—a small molecule recognized by the CLIP-tag. Similarly to SNAP$_f$, the CLIP$_f$ sequence specifically recognizes derivatives prepared from BC-amine. As a result of this reaction, the labeled exogenous protein EGF-CLIP$_f$-ATTO647N was formed. During incubation of EGFR-SNAP$_f$-Chromeo494 with EGF-CLIP$_f$-ATTO647N, EGF specifically binds to EGFR. This resulted in the double staining of the EGFR-EGF complex with two dyes suitable for two-color STED imaging (figure 15).

Imaging was performed by sequential excitation of the fluorophores with synchronized pulsed lasers at 532 nm (for Chromeo™ 494) and 640 nm (for ATTO647N) and depletion with a tunable mode locked Ti : sapphire laser at 760 nm. Depletion with a commercial 775 nm STED laser is also possible, as it was showed for these dyes separately. A time series of STED images (see figure 15) showed that shortly after EGF stimulation, an endosome-like structure containing ATTO674N label began to form. This result was the first example of two-color live cell STED imaging and showed that STED microscopy has a great potential in revealing the biologically relevant processes in living cells. However, it is important to note that EGF is an extracellular protein and EGFR is a cell-surface receptor, and only therefore it was possible to label their CLIP and SNAP fusions with *cell impermeable* BC-ATTO647N and BG-Chromeo™ 494 markers. Cell permeability of the markers is an important prerequisite for the intracellular labeling of living cells, and not many fluorescent dyes are known to be cell-permeable.

In another study, the coumarin dye DY-480XL (for structure, see table 1) with a large Stokes shift and with optical spectra similar to those of DY-485XL was used together with a red-emitting rhodamine dye KK114 [116–118]. These dyes were used in the investigation of the spatial organization of the synaptotagmin 1 (Syt1) surface pool in hippocampal presynaptic boutons [119]. For that, dual-color isoSTED microscopy was used. In order to reveal the localization of surface-stranded Syt1 at synapses, Syt1 was immunostained with KK114 dye. The synapses were identified by labeling pre- and postsynaptic markers RIM1, RIM2 (RIM) and Homer1 with the coumarin dye DY-480XL. These flurophores were excited separately at fixed wavelengths of 530 nm (for DY-480XL) and 635 nm (for KK114). Both dyes have similar emission spectra, and in order to achieve nanoscale resolution, STED pulses only at one wavelength of 775 nm were sufficient. Emission of both fluorophores was detected in the range of 660 − 700 nm (in separate channels coupled with two distinct excitation modes). After deconvolution, the final super-resolved images were obtained (figure 16).

Another large Stokes shift dye, Abberior Star 520 SXP, together with a 'normal' red-emitting fluorochrome Abberior Star 635 was used in a dual-color STED imaging experiment which allowed the assessment of the localization of collagen I (an abundant component of the extracellular matrix) within Golgi ministacks upon treatment with nocodazole and showed that collagen I is retained at the *cis* face (figure 17) [120]. This result led the authors to a conclusion that the flow of collagen through the Golgi ministack was inhibited.

Conclusion and outlook

Table 1 contains commercial fluorescent dyes and their spectral properties which, in most cases, are compatible with the depletion wavelengths available in STED microscopes produced by LEICA Microsytems, Abberior Instruments and Picoquant GmbH. All published examples have been discussed in the text, but there are many more promising dyes with large Stokes shifts (e.g. calcium indicators *Indo 1* and *Fura 2*) which have not yet been applied in STED microscopy (and other super-resolution methods). In this respect, table 1 may be helpful in choosing the suitable fluorescent marker with large Stokes shift as a 'second' or even 'third' dye in a set of light-emitting labels for multicolor super-resolution imaging. Table 1 contains the structures of the dyes (if these are known) and provides useful chemical evidence for creating brighter and more photostable fluorophores. In particular, it becomes clear that not only the coumarin dyes are promising development candidates. For example, pyrene dyes are expected to be more photostable than the coumarins. However, they still require new chemical transformations and non-trivial substituents amplifying electronic 'push–pull' effects and, as a result, increasing extinction coefficients, fluorescent quantum yields (thus improving brightness) and shifting of the emission (and, to a lesser extent, absorption) bands to the red spectral region.

New and efficient tools of dye design, 'modular' approaches and flexible synthetic routes to fluorophores with required spectral properties have been invented in recent years. We can expect that these achievements will result in more photostable and bright dyes with large Stokes shifts. It is already clear now that super-resolution optical microscopy is very powerful tool in life sciences and medicine. Therefore, biology, medicine and material sciences may be considered as the source and the main driving force for future discoveries, in which optical nanoscopy is expected to play a key role.

References

[1] Eggeling C and Hell S W 2015 STED fluorescence nanoscopy *Far-Field Optical Nanoscopy* ed P Tinnefeld *et al* (Berlin: Springer) pp 3–25

[2] Gould T J, Pellett P A and Bewersdorf J 2013 STED microscopy *Fluorescence Microscopy: From Principles to Biological Applications* ed U Kubitscheck (Weinheim: Wiley-VCH) pp 375–92

[3] Yushchenko D A and Bruchez M P 2015 Tailoring fluorescent labels for far-field nanoscopy *Far-Field Optical Nanoscopy* ed P Tinnefeld *et al* (Berlin: Springer) pp 159–88

[4] Hell S W 2003 Toward fluorescence nanoscopy *Nat. Biotechnol.* **21** 1347–55

[5] Wurm C A, Neumann D, Schmidt R, Egner A and Jakobs S 2010 Sample preparation for STED microscopy *Live Cell Imaging* ed D B Papkovsky (New York: Humana Press) pp 185–99

[6] Rankin Brian R, Moneron G, Wurm Christian A, Nelson Jessica C, Walter A, Schwarzer D, Schroeder J, Colón-Ramos Daniel A and Hell S W 2011 Nanoscopy in a living multicellular organism expressing GFP *Biophys. J.* **100** L63–L5

[7] Jost A and Heintzmann R 2013 Superresolution multidimensional imaging with structured illumination microscopy *Annu. Rev. Mater. Res.* **43** 261–82

[8] Allen J R, Ross S T and Davidson M W 2014 Structured illumination microscopy for superresolution *ChemPhysChem* **15** 566–76

[9] Gonçalves M S T 2009 Fluorescent labeling of biomolecules with organic probes *Chem. Rev.* **109** 190–212

[10] Lippincott-Schwartz J, Snapp E and Kenworthy A 2001 Studying protein dynamics in living cells *Nat. Rev. Mol. Cell. Biol.* **2** 444–56

[11] Lidke D S and Wilson B S 2009 Caught in the act: quantifying protein behaviour in living cells *Trends Cell Biol.* **19** 566–74

[12] Sauer M, Hofkens J and Enderlein J 2011 *Handbook of Fluorescence Spectroscopy and Imaging* (Weinheim: Wiley-VCH)

[13] Fernandez-Suarez M and Ting A Y 2008 Fluorescent probes for super-resolution imaging in living cells *Nat. Rev. Mol. Cell Biol.* **9** 929–43

[14] Patterson G, Davidson M, Manley S and Lippincott-Schwartz J 2010 Superresolution imaging using single-molecule localization *Annu. Rev. Phys. Chem.* **61** 345–67

[15] Petchprayoon C, Yan Y, Mao S and Marriott G 2011 Rational design, synthesis, and characterization of highly fluorescent optical switches for high-contrast optical lock-in detection (OLID) imaging microscopy in living cells *Bioorg. Med. Chem.* **19** 1030–40

[16] Stennett E M, Ciuba M A and Levitus M 2014 Photophysical processes in single molecule organic fluorescent probes *Chem. Soc. Rev.* **43** 1057–75

[17] Chozinski T J, Gagnon L A and Vaughan J C 2014 Twinkle, twinkle little star: photoswitchable fluorophores for super-resolution imaging *FEBS Lett.* **588** 3603–12

[18] Umezawa K, Citterio D and Suzuki K 2014 New trends in near-infrared fluorophores for bioimaging *Anal. Sci.* **30** 327–49

[19] Peters R 2013 Fluorescence photobleaching and photoactivation techniques *Fluorescence Microscopy: from Principles to Biological Applications* ed U Kubitscheck (Weinheim: Wiley-VCH) pp 215–44

[20] Raymo F M 2013 Photoactivatable synthetic fluorophores *Phys. Chem. Chem. Phys.* **15** 14840–50

[21] Raymo F M 2012 Photoactivatable synthetic dyes for fluorescence imaging at the nanoscale *J. Phys. Chem. Lett.* **3** 2379–85

[22] Sauer M 2013 Localization microscopy coming of age: from concepts to biological impact *J. Cell. Sci.* **126** 3505–13

[23] Furstenberg A and Heilemann M 2013 Single-molecule localization microscopy-near-molecular spatial resolution in light microscopy with photoswitchable fluorophores *Phys. Chem. Chem. Phys.* **15** 14919–30

[24] Finan K, Flottmann B and Heilemann M 2013 Photoswitchable fluorophores for single-molecule localization microscopy *Methods Mol. Biol.* **950** 131–51

[25] Grimm J B, Heckman L M and Lavis L D 2013 The chemistry of small-molecule fluorogenic probes *Prog. Mol. Biol. Transl. Sci.* **113** 1–34

[26] Li W-H and Zheng G 2012 Photoactivatable fluorophores and techniques for biological imaging applications *Photochem. Photobiol. Sci.* **11** 460–71

[27] van de Linde S and Sauer M 2014 How to switch a fluorophore: from undesired blinking to controlled photoswitching *Chem. Soc. Rev.* **43** 1076–87

[28] Grimm J B, Sung A J, Legant W R, Hulamm P, Matlosz S M, Betzig E and Lavis L D 2013 Carbofluoresceins and carborhodamines as scaffolds for high-contrast fluorogenic probes *ACS Chem. Biol.* **8** 1303–10

[29] Ragab S S, Swaminathan S, Baker J D and Raymo F M 2013 Activation of BODIPY fluorescence by the photoinduced dealkylation of a pyridinium quencher *Phys. Chem. Chem. Phys.* **15** 14851–5

[30] Aotake T, Tanimoto H, Hotta H, Kuzuhara D, Okujima T, Uno H and Yamada H 2013 *In situ* preparation of highly fluorescent pyrene-dyes from non-luminous precursors upon photoirradiation *Chem. Commun.* **49** 3661–3

[31] Grimm J B *et al* 2015 A general method to improve fluorophores for live-cell and single-molecule microscopy *Nat. Methods* **12** 244–50

[32] Lukinavicius G *et al* 2013 A near-infrared fluorophore for live-cell super-resolution microscopy of cellular proteins *Nat. Chem.* **5** 132–9

[33] Lukinavicius G *et al* 2014 Fluorogenic probes for live-cell imaging of the cytoskeleton *Nat. Methods* **11** 731–3

[34] Godin A G, Lounis B and Cognet L 2014 Super-resolution Microscopy Approaches for Live Cell Imaging *Biophys. J.* **107** 1777–84

[35] Hermanson G T 2013 *Bioconjugate Techniques* (Amsterdam: Elsevier)

[36] Vira S, Mekhedov E, Humphrey G and Blank P S 2010 Fluorescent-labeled antibodies: Balancing functionality and degree of labeling *Anal. Biochem.* **402** 146–50

[37] Härtig W and Fritschy J-M 2009 Immunofluorescence: dyes and other haptens conjugated with antibodies *eLS* (Hoboken, NJ: Wiley)

[38] Buchwalow I B and Böcker W 2010 Antibody labeling and the choice of the label *Immunohistochemistry: Basics and Methods* (Berlin: Springer) pp 9–17

[39] Mao S-Y and Mullins J M 2010 Conjugation of fluorochromes to antibodies *Immunocytochemical Methods and Protocols* ed C Oliver and M C Jamur (New York: Humana Press) pp 43–8

[40] Odell I D and Cook D 2013 Immunofluorescence techniques *J. Invest. Dermatol.* **133** e4

[41] Petchprayoon C, Suwanborirux K, Tanaka J, Yan Y, Sakata T and Marriott G 2005 Fluorescent kabiramides: new probes to quantify actin *in vitro* and *in vivo Bioconjugate Chem.* **16** 1382–9

[42] Sauer M 2015 A practical guide to dSTORM: super-resolution imaging with standard fluorescent probes *Far-Field Optical Nanoscopy* ed P Tinnefeld *et al* (Berlin: Springer) pp 65–84

[43] Muyldermans S 2013 Nanobodies: natural single-domain antibodies *Annu. Rev. Biochem.* **82** 775–97

[44] Ries J, Kaplan C, Platonova E, Eghlidi H and Ewers H 2012 A simple, versatile method for GFP-based super-resolution microscopy via nanobodies *Nat. Methods* **9** 582–4

[45] Grußmayer K S, Kurz A and Herten D-P 2014 Single-molecule studies on the label number distribution of fluorescent markers *ChemPhysChem* **15** 734–42

[46] Schnell U, Dijk F, Sjollema K A and Giepmans B N 2012 Immunolabeling artifacts and the need for live-cell imaging *Nat. Methods* **9** 152–8

[47] Gronemeyer T, Godin G and Johnsson K 2005 Adding value to fusion proteins through covalent labelling *Curr. Opin. Biotechnol.* **16** 453–8

[48] Sun X *et al* 2011 Development of SNAP-tag fluorogenic probes for wash-free fluorescence imaging *ChemBioChem* **12** 2217–26

[49] Keppler A, Gendreizig S, Gronemeyer T, Pick H, Vogel H and Johnsson K 2003 A general method for the covalent labeling of fusion proteins with small molecules *in vivo Nat. Biotechnol.* **21** 86–9

[50] Keppler A, Pick H, Arrivoli C, Vogel H and Johnsson K 2004 Labeling of fusion proteins with synthetic fluorophores in live cells *Proc. Natl Acad. Sci. USA* **101** 9955–9

[51] Zhao W, Ding Y and Xia Q 2011 Time-dependent density functional theory study on the absorption spectrum of Coumarin 102 and its hydrogen-bonded complexes *J. Comput. Chem.* **32** 545–53
[52] Los G V *et al* 2008 HaloTag: a novel protein labeling technology for cell imaging and protein analysis *ACS Chem. Biol.* **3** 373–82
[53] Hsieh C-C, Ho M-L and Chou P-T 2010 Organic dyes with excited-state transformations (electron, charge, and proton transfers) *Advanced Fluorescence Reporters in Chemistry and Biology I* ed A P Demchenko (Berlin: Springer) pp 225–66
[54] Lang K and Chin J W 2014 Cellular incorporation of unnatural amino acids and bioorthogonal labeling of proteins *Chem. Rev.* **114** 4764–806
[55] Jie W, Jie L, Yi Y, Maiyun Y and Peng R C 2014 Small-molecule labeling probes *Optical Nanoscopy and Novel Microscopy Techniques* (Boca Raton, FL: CRC Press) pp 85–110
[56] Nikic I, Plass T, Schraidt O, Szymanski J, Briggs J A, Schultz C and Lemke E A 2014 Minimal tags for rapid dual-color live-cell labeling and super-resolution microscopy *Angew. Chem. Int. Ed. Engl.* **53** 2245–9
[57] Dumas A, Lercher L, Spicer C D and Davis B G 2015 Designing logical codon reassignment—expanding the chemistry in biology *Chem. Sci.* **6** 50–69
[58] Deng B, Lin Y, Wang C, Li F, Wang Z, Zhang H, Li X-F and Le X C 2014 Aptamer binding assays for proteins: the thrombin example—a review *Anal. Chim. Acta* **837** 1–15
[59] Opazo F, Levy M, Byrom M, Schafer C, Geisler C, Groemer T W, Ellington A D and Rizzoli S O 2012 Aptamers as potential tools for super-resolution microscopy *Nat. Methods* **9** 938–9
[60] Eggeling C, Widengren J, Rigler R and Seidel C A M 1998 Photobleaching of fluorescent dyes under conditions used for single-molecule detection: evidence of two-step photolysis *Anal. Chem.* **70** 2651–9
[61] Hell S W 2010 Far-field optical nanoscopy *Single Molecule Spectroscopy in Chemistry, Physics and Biology* ed A Gräslund *et al* (Berlin: Springer) pp 365–98
[62] Puliti D, Warther D, Orange C, Specht A and Goeldner M 2011 Small photoactivatable molecules for controlled fluorescence activation in living cells *Bioorg. Med. Chem.* **19** 1023–9
[63] van de Linde S, Wolter S and Sauer M 2011 Single-molecule photoswitching and localization *Austr. J. Chem.* **64** 503–11
[64] Muller T, Schumann C and Kraegeloh A 2012 STED microscopy and its applications: new insights into cellular processes on the nanoscale *ChemPhysChem* **13** 1986–2000
[65] Liu X, Xu Z and Cole J M 2013 Molecular design of UV–vis absorption and emission properties in organic fluorophores: toward larger bathochromic shifts, enhanced molar extinction coefficients, and greater stokes shifts *J. Phys. Chem.* C **117** 16584–95
[66] Vollmer F, Rettig W and Birckner E 1994 Photochemical mechanisms producing large fluorescence stokes shifts *J. Fluoresc.* **4** 65–9
[67] Jones G II, Jackson W R and Halpern A M 1980 Medium effects on fluorescence quantum yields and lifetimes for coumarin laser dyes *Chem. Phys. Lett.* **72** 391–5
[68] Jones G II, Jackson W R, Kanoktanaporn S and Halpern A M 1980 Solvent effects on photophysical parameters for coumarin laser dyes *Opt. Commun.* **33** 315–20
[69] Jones G, Jackson W R, Choi C Y and Bergmark W R 1985 Solvent effects on emission yield and lifetime for coumarin laser dyes. Requirements for a rotatory decay mechanism *J. Phys. Chem.* **89** 294–300
[70] Grandberg I I, Denisov L K and Popova O A 1987 7-Aminocoumarins (Review) *Chem. Heterocycl. Compd.* **23** 117–42
[71] Reynolds G A and Drexhage K H 1975 New coumarin dyes with rigidized structure for flashlamp-pumped dye lasers *Opt. Commun.* **13** 222–5
[72] Drexhage K H, Erikson G R, Hawks G H and Reynolds G A 1975 Water-soluble coumarin dyes for flashlamp-pumped dye lasers *Opt. Commun.* **15** 399–403
[73] Fletcher A N, Bliss D E and Kauffman J M 1983 Lasing and fluorescent characteristics of nine, new, flashlamp-pumpable, coumarin dyes in ethanol and ethanol: water *Opt. Commun.* **47** 57–61
[74] Corrie J E T, Munasinghe V R N and Rettig W 2000 Synthesis and fluorescence properties of substituted 7-aminocoumarin-3-carboxylate derivatives *J. Heterocycl. Chem.* **37** 1447–55
[75] Uttamapinant C, White K A, Baruah H, Thompson S, Fernández-Suárez M, Puthenveetil S and Ting A Y 2010 A fluorophore ligase for site-specific protein labeling inside living cells *Proc. Natl. Acad. Sci. USA* **107** 10914–9
[76] Lin Q N, Bao C Y, Fan G S, Cheng S Y, Liu H, Liu Z Z and Zhu L Y 2012 7-Amino coumarin based fluorescent phototriggers coupled with nano/bio-conjugated bonds: synthesis, labeling and photorelease *J. Mater. Chem.* **22** 6680–8
[77] Gordo J, Avó J, Parola A J, Lima J C, Pereira A and Branco P S 2011 Convenient synthesis of 3-vinyl and 3-styryl coumarins *Org. Lett.* **13** 5112–5
[78] Murata C, Masuda T, Kamochi Y, Todoroki K, Yoshida H, Nohta H, Yamaguchi M and Takadate A 2005 Improvement of fluorescence characteristics of coumarins: syntheses and fluorescence properties of 6-methoxycoumarin and benzocoumarin derivatives as novel fluorophores emitting in the longer wavelength region and their application to analytical reagents *Chem. Pharm. Bull.* **53** 750–8
[79] 2010 *The Molecular Probes Handbook: A Guide to Fluorescent Probes and Labeling Technologies* ed I Johnson *et al* (Life Technologies)
[80] Schiedel M-S, Briehn C A and Bäuerle P 2001 Single-compound libraries of organic materials: parallel synthesis and screening of fluorescent dyes *Angew. Chem. Int. Ed. Engl.* **40** 4677–80
[81] Gordeeva N A, Kirpichenok M A, Patalakha N S and Grandberg I I 1990 Synthesis, spectral-luminescence, and acid-base properties of 3-halo-7-aminocoumarins *Chem. Heterocycl. Compd.* **26** 1329–37
[82] Ehrenschwender T, Varga B R, Kele P and Wagenknecht H-A 2010 New far-red and near-infrared fluorescent probes with large stokes shifts for dual covalent labeling of DNA *Chem. Asian J.* **5** 1761–4
[83] Nagy K, Orban E, Bosze S and Kele P 2010 Clickable long-wave 'Mega-Stokes' fluorophores for orthogonal chemoselective labeling of cells *Chem. Asian J.* **5** 773–7
[84] Richard J-A, Massonneau M, Renard P-Y and Romieu A 2008 7-Hydroxycoumarin – hemicyanine hybrids: a new class of far-red emitting fluorogenic dyes *Org. Lett.* **10** 4175–8
[85] Huang H-C, Wang K-L, Huang S-T, Lin H-Y and Lin C-M 2011 Development of a sensitive long-wavelength fluorogenic probe for nitroreductase: a new fluorimetric indictor for analyte determination by dehydrogenase-coupled biosensors *Biosens. Bioelectron.* **26** 3511–6
[86] Huang S-T, Peng Y-X and Wang K-L 2008 Synthesis of a new long-wavelength latent fluorimetric indicator for analytes determination in the DT-Diaphorase coupling dehydrogenase assay system *Biosens. Bioelectron.* **23** 1793–8
[87] Huang S-T, Ting K-N and Wang K-L 2008 Development of a long-wavelength fluorescent probe based on quinone–methide-type reaction to detect physiologically significant thiols *Anal. Chim. Acta* **620** 120–6
[88] Li H, Cai L and Chen Z 2012 Coumarin-derived fluorescent chemosensors *Advances in Chemical Sensors* ed W Wang (Rijeka: InTech) pp 121–50
[89] Kim E and Park S 2010 Discovery of new fluorescent dyes: targeted synthesis or combinatorial approach? *Advanced Fluorescence Reporters in Chemistry and Biology I* ed A P Demchenko (Berlin: Springer) pp 149–86
[90] Nizamov S, Willig K I, Sednev M V, Belov V N and Hell S W 2012 Phosphorylated 3-heteroarylcoumarins and their use in fluorescence microscopy and nanoscopy *Chem. Eur. J.* **18** 16339–48
[91] Schill H, Nizamov S, Bottanelli F, Bierwagen J, Belov V N and Hell S W 2013 4-Trifluoromethyl-substituted coumarins with large stokes shifts: synthesis, bioconjugates, and their use in super-resolution fluorescence microscopy *Chem. Eur. J.* **19** 16556–65
[92] Fletcher A N and Bliss D E 1978 Laser dye stability. Part 5 *Appl. Phys.* **16** 289–95

[93] Sun W-C, Gee K R and Haugland R P 1998 Synthesis of novel fluorinated coumarins: excellent UV-light excitable fluorescent dyes *Bioorg. Med. Chem. Lett.* **8** 3107–10
[94] Jin X, Uttamapinant C and Ting A Y 2011 Synthesis of 7-aminocoumarin by Buchwald–Hartwig cross coupling for specific protein labeling in living cells *ChemBioChem* **12** 65–70
[95] Czerney P, Wenzel M, Schweder B and Lehmann F 2009 *US Patent* 756390
[96] Rechthaler K and Köhler G 1994 Excited state properties and deactivation pathways of 7-aminocoumarins *Chem. Phys.* **189** 99–116
[97] Donnert G, Keller J, Wurm C A, Rizzoli S O, Westphal V, Schönle A, Jahn R, Jakobs S, Eggeling C and Hell S W 2007 Two-color far-field fluorescence nanoscopy *Biophys. J.* **92** L67–L9
[98] Rankin B R, Kellner R R and Hell S W 2008 Stimulated-emission-depletion microscopy with a multicolor stimulated-Raman-scattering light source *Opt. Lett.* **33** 2491–3
[99] Westphal V, Rizzoli S O, Lauterbach M A, Kamin D, Jahn R and Hell S W 2008 Video-rate far-field optical nanoscopy dissects synaptic vesicle movement *Science* **320** 246–9
[100] Friedemann K, Turshatov A, Landfester K and Crespy D 2011 Characterization via two-color STED microscopy of nanostructured materials synthesized by colloid electrospinning *Langmuir* **27** 7132–9
[101] Mace E M and Orange J S 2012 Dual channel STED nanoscopy of lytic granules on actin filaments in natural killer cells *Commun. Integr. Biol.* **5** 184–6
[102] Henkel B, Drose D R, Ackels T, Oberland S, Spehr M and Neuhaus E M 2014 Co-expression of anoctamins in cilia of olfactory sensory neurons *Chem. Senses* **40** 73–87
[103] Westin L, Reuss M, Lindskog M, Aperia A and Brismar H 2014 Nanoscopic spine localization of Norbin, an mGluR5 accessory protein *BMC Neurosci.* **15** 45
[104] Johnson A, Bhattacharya N, Hanna M, Pennington J G, Schuh A L, Wang L, Otegui M S, Stagg S M and Audhya A 2015 TFG clusters COPII-coated transport carriers and promotes early secretory pathway organization *The EMBO J.* **34** 811–27
[105] Olson J P, Banghart M R, Sabatini B L and Ellis-Davies G C R 2013 Spectral evolution of a photochemical protecting group for orthogonal two-color uncaging with visible light *J. Am. Chem. Soc.* **135** 15948–54
[106] Bianchini P, Peres C, Oneto M, Galiani S, Vicidomini G and Diaspro A 2015 STED nanoscopy: a glimpse into the future *Cell Tissue Res.* **360** 143–50
[107] Wang I H, Suomalainen M, Andriasyan V, Kilcher S, Mercer J, Neef A, Luedtke Nathan W and Greber Urs F 2013 Tracking viral genomes in host cells at single-molecule resolution *Cell Host Microbe* **14** 468–80
[108] Clausen M P, Galiani S, Serna J B d l, Fritzsche M, Chojnacki J, Gehmlich K, Lagerholm B C and Eggeling C 2014 Pathways to optical STED microscopy *NanoBioImaging* **1** doi: 10.2478/nbi-2013-0001
[109] Okada Y and Nakagawa S 2015 Super-resolution imaging of nuclear bodies by STED microscopy *Nuclear Bodies and Noncoding RNAs* ed S Nakagawa and T Hirose (New York: Springer) pp 21–35
[110] Schmidt R, Wurm C A, Jakobs S, Engelhardt J, Egner A and Hell S W 2008 Spherical nanosized focal spot unravels the interior of cells *Nat. Methods* **5** 539–44
[111] Dean C *et al* 2012 Distinct subsets of Syt-IV/ BDNF vesicles are sorted to axons versus dendrites and recruited to synapses by activity *J. Neurosci.* **32** 5398–413
[112] Kempf C, Staudt T, Bingen P, Horstmann H, Engelhardt J, Hell S W and Kuner T 2013 Tissue multicolor STED nanoscopy of presynaptic proteins in the calyx of held *PLoS One* **8** e62893
[113] Wilfling F *et al* 2014 Arf1/COPI machinery acts directly on lipid droplets and enables their connection to the ER for protein targeting *eLife* **3** e01607
[114] Karlsson T, Turkina M V, Yakymenko O, Magnusson K-E and Vikström E 2012 The *Pseudomonas aeruginosa* N-acylhomoserine lactone quorum sensing molecules target IQGAP1 and modulate epithelial cell migration *PLoS Pathog.* **8** e1002953
[115] Pellett P A, Sun X, Gould T J, Rothman J E, Xu M-Q, Corrêa I R and Bewersdorf J 2011 Two-color STED microscopy in living cells *Biomed. Opt. Express* **2** 2364–71
[116] Kolmakov K, Belov V N, Bierwagen J, Ringemann C, Müller V, Eggeling C and Hell S W 2010 Red-emitting rhodamine dyes for fluorescence microscopy and nanoscopy *Chem. Eur. J.* **16** 158–66
[117] Wurm C *et al* 2012 Novel red fluorophores with superior performance in STED microscopy *Opt. Nanoscopy* **1** 7
[118] Kolmakov K, Wurm C A, Meineke D N H, Göttfert F, Boyarskiy V P, Belov V N and Hell S W 2014 Polar red-emitting rhodamine dyes with reactive groups: synthesis, photophysical properties, and two-color STED nanoscopy applications *Chem. Eur. J.* **20** 146–57
[119] Hua Y F, Sinha R, Thiel C S, Schmidt R, Huve J, Martens H, Hell S W, Egner A and Klingauf J 2011 A readily retrievable pool of synaptic vesicles *Nat. Neurosci.* **14** 833–9
[120] Lavieu G, Dunlop M H, Lerich A, Zheng H, Bottanelli F and Rothman J E 2014 The Golgi ribbon structure facilitates anterograde transport of large cargoes *Mol. Biol. Cell* **25** 3028–36